https://ntrs.nasa.gov/search.jsp?R=19730012445 2020-03-23T02:34:10+00:00Z

N73-21172

UNIVERSITY OF ILLINOIS
URBANA

CASE FILE
COPY

AERONOMY REPORT NO. 52

PRELIMINARY DESIGN STUDY OF A HIGH-RESOLUTION METEOR RADAR

by
W. Lee
M. A. Geller

March 1, 1973

Supported by
National Aeronautics and Space Administration
Grant NGR 14-005-181

Aeronomy Laboratory
Department of Electrical Engineering
University of Illinois
Urbana, Illinois

CITATION POLICY

The material contained in this report is preliminary information circulated rapidly in the interest of prompt interchange of scientific information and may be later revised on publication in accepted aeronomic journals. It would therefore be appreciated if persons wishing to cite work contained herein would first contact the authors to ascertain if the relevant material is part of a paper published or in process.

UILU-Eng-73-2502

A E R O N O M Y R E P O R T

N O. 52

PRELIMINARY DESIGN STUDY OF A HIGH-RESOLUTION METEOR RADAR

by

W. Lee
M. A. Geller

March 1, 1973

Supported by
National Aeronautics and
Space Administration
Grant NGR 14-005-181

Aeronomy Laboratory
Department of Electrical Engineering
University of Illinois
Urbana, Illinois

ABSTRACT

A design study for a high-resolution meteor radar system is carried out with the objective of measuring upper atmospheric winds and particularly studying short period atmospheric waves in the 80 to 120 km altitude region. The transmitter that is to be used emits a peak power of 4 Mw. The system is designed to measure the wind velocity and height of a meteor trail very accurately. This is achieved using a specially developed digital reduction procedure to determine wind velocity and range together with an interferometer for measuring both the azimuth and elevation angles of the region with a long baseline vernier measurement being used to refine the elevation angle measurement. The resultant accuracies are calculated to be $\pm$ 0.9 m/s for the wind, $\pm$ 230 m for the range and $\pm$ 0.12° for the elevation angle, giving a height accuracy of $\pm$ 375 m. The prospects for further development of this system are also discussed.

TABLE OF CONTENTS

LIST OF FIGURES

1. INTRODUCTION

Many meteors of various sizes enter the earth's atmosphere and burn up each day, leaving ionized trails in their path. The larger trails can be seen with the naked eye, but even the smaller meteors (down to 15th magnitude), which are more common, leave trails that provide radar targets around 40 MHz. These provide a very large number of meteor trails that are detectable by radio means. It has been estimated [*Manning and Eshleman*, 1959] that meteors above the 15th magnitude occur at a rate of about 160 per square meter per second. This figure is given for the sporadic meteors and does not include the contributions of showers.

Most of these meteors are not detected since specular reflection from a meteor trail is required for a radar echo to be received. In other words, the meteor trail must be oriented at right angles to the radar beam, and the principal contribution to the echo power comes from the first Fresnel zone around the specular reflection point. Since only a small percentage of the meteor trails are detected, a radar beam should be pointed in the direction where specular reflection occurs most often. This direction varies with the time of day. For example, in the Northern Hemisphere maximum echo rates occur to the north at 6 a.m., to the east at 12 noon, to the south at 6 p.m., and to the west at 12 midnight [*Villard et al.*, 1955].

After the development of radar in World War II, studies of meteors were started using this technique and researchers began to concentrate on explaining the physical characteristics of meteor echoes. Most of these studies are summarized in a book by *McKinley* [1961]. Since then, meteor trails have been used to explore the earth's atmosphere in the height region from 80 to 120 km.

The proposed meteor radar system described herein is a further step in the exploration of the atmosphere.

1.1 *Atmospheric Winds*

Since the kinematic viscosity increases with height in the atmosphere, there is an appreciable drag between the different layers. Thus up to heights well above 100 km, the whole atmosphere participates in the earth's rotation.

Under the equilibrium of gravity, pressure, and the Coriolis force in this rotating atmosphere, a geostrophic wind system results. In meteor radar studies, this wind is also called the prevailing wind. The prevailing wind comprises two distinct components, a zonal mean wind and contributions from planetary waves. Superimposed on these winds are tidal wind motions. A 24-hour component, called the solar diurnal tide, is a superposition of many modes forced by solar heating of water vapor and ozone, some of these modes being evanescent while others are propagating. A 12-hour component, called the solar semidiurnal tide, is found to be essentially one very long wavelength propagating mode that is forced principally by solar heating of ozone and water vapor. This semidiurnal tide tends to dominate the diurnal tide at higher latitudes than 30°. Another shorter-vertical-wavelength semidiurnal mode may dominate above 80 km during some seasons [*Chapman and Lindzen*, 1970]. Tidal modes of 8-hour and 6-hour periods have also been determined [*Muller*, 1970].

Under normal conditions turbulence dominates vertical-transport processes in the mesosphere and lower thermosphere. There have been a number of measurements of atmospheric turbulent parameters, especially by the observation of rocket vapor releases. The most prominent feature of these observations is the cessation of turbulence above about 105 km, this level being described

as the turbopause. From the rate of expansion of vapor trails below this altitude, it has been suggested that the eddy diffusion coefficient is between 10^6-10^7 cm^2/sec [*Justus*, 1967]. Whether this value represents the action of true small-scale isotropic turbulence or the diffusive action of the larger scale motions is not yet clear.

In 1960 Hines proposed the existence of gravity waves. A comprehensive picture is envisaged for the motions normally encountered, in which a spectrum of gravity waves is generated at low levels of the atmosphere and propagates upward. Sources suggested for naturally-occurring gravity waves have included earthquakes, oscillations in stratospheric jet streams, air flow over motions, solar eclipses, hurricanes, thunderstorms, and many more. The propagational effects of amplification, reflection, intermodulation, and dissipation act to change the spectrum continuously with increasing height, and so produce different types of dominant modes at different heights. These changes serve to explain much of the irregular motions and ionization perturbations in the mesosphere and thermosphere. The observational work on gravity waves is presently lagging badly behind theory. This situation should be remedied by systematic programs of observations.

1.2 *Survey of Methods*

Conceptually, atmospheric measurements are obtained most simply with probes placed directly into the medium. This method is done traditionally with radiosondes in the lower atmosphere where probes can be supported by balloons whose upper limit is approximately 30 km. Due to the development of sounding balloons and meteorological rockets, the study of the wind structure of the atmosphere up to about 60 km has been quite extensive throughout certain areas of the world. Above this height, instruments such as grenades,

pitot tubes and falling spheres, can be placed only by larger rockets. This is expensive and probes cannot remain aloft very long.

Another approach uses the passive probe. For example, clouds of chemicals can be released in the upper atmosphere by rockets or by gun-launched projectiles. Tracking the movement and distortion of these clouds provides information on the wind structure at a given time and place. Mean winds, however, are very hard to measure from such trails. Measurement of wind by any of these rocket methods is very expensive. The need for some continuous ground-based observations has been acutely felt.

Some of these passive probes are actually supplied by nature. Historically, one of the oldest methods of wind measurement used the observation of noctilucent clouds [*Mitra*, 1947]. Because observations are only possible during twilight and the occurrence of these clouds is not predictable, this method is limited. *Mitra* [1949] pioneered a method in which the movements of ionospheric irregularities can be tracked by radio measurements from the ground. The method is still being used extensively, but the interpretation of the fading records and the velocities obtained therefrom are not clearly understood. One of the main reasons for this difficulty is the uncertainty about the fading mechanism. A recent work by *Guha and Geller* [1972] examines the methods of measuring ionospheric drift from fading records in order to see their applicability and validity.

Meteor trails can be viewed as another type of passive probe. It has been shown that these trails move with the surrounding neutral atmosphere [*Manning et al.*, 1950] and, therefore, winds can be determined from the observed Doppler shifts. The techniques developed so far are able to yield information continuously throughout the whole day. The complexity of meteor

radar stations increases when heights of the observed drifts are being determined. Not only do the amplitude and the Doppler shift of the received signal have to be measured but also the range and the angle of arrival of the signal. Often several antennas and receivers are used for this purpose, and many measured values are recorded synchronously. In comparison to the rocket experiments, however, the costs of these investigations are relatively small. Also, unlike the rocket methods, the meteor radar technique is able to monitor the meteor region continuously.

Other measurement approaches have been used and are being developed. Ionospheric motion has been measured by observing the velocity of the diffraction pattern formed on the ground by radio waves partially reflected from the region between 65 and 100 km [*Fraser*, 1967]. However, in the height region between 80 and 120 km, the potential of the meteor-trail method for almost continuous acquisition of data on winds, at low cost, makes it a very promising tool for exploring the atmosphere. This method has yielded an impressive amount of information on atmospheric parameters and will do more.

2. SURVEY OF METEOR WIND SYSTEMS

The first determinations of wind velocity in the altitude region around 90 km by means of radio reflections from meteor trails were undertaken at Stanford University by *Manning et al.* [1950]. Since that time, the technique was brought into regular use at Adelaide, Australia [*Elford and Robertson*, 1953] and at Jodrell Bank, England [*Greenhow*, 1954]. Their observations were of winds averaged over the altitude region 80-100 km. Work at Stanford was discontinued because of the great amount of data that had been processed by hand. The Jodrell Bank facility has also ceased operation. At Adelaide meteor wind studies are still continuing. The Adelaide facility will be described in Section 2.4. Several stations have been built in Russia which resemble that at Jodrell Bank. In 1966 a workshop on methods of obtaining winds from meteor trails was held in Waltham, Massachusetts [*Barnes and Pazniokas*, 1968]. Six meteor radar systems were represented at the workshop. A list of them and their characteristics is given in Table 2.1 [*Barnes*, 1968]. It is the purpose of this survey to describe these six systems and their changes since the workshop. The Havana system has been disbanded, and the transmitter and parts of the receiving equipment are being used to construct the new facility at the University of Illinois.

2.1 *Stanford Meteor-Trails Radar*

The Stanford Meteor Radar is a phase-coherent one-station pulse system. The operating frequency is 30.14 MHz and the transmitter has a peak power of 5 kW. The system was built with an eye toward low cost, easy mobility and simple rugged construction for unattended operation. Winds are measured from the Doppler shift of the meteor echo. The height of an echo is determined by

TABLE 2.1

Data on the six operating meteor trail wind sets represented at the Workshop (August 1966).

Station	Power	Frequency (MHz)	Approximate Location	Minimum Hourly Rate	Cost Ratio	Height Accuracy (km)
Havana, Illinois United States	3 MW pulse	40.92	40N, 90W	(500)	10+	± 3
Adelaide, South Australia	1.5 kW cw	26.8	35S, 139E	30	2	± 2
Garchy Cher, France	5 kW cw	30	47N, 3E	10-20	1.5	± 3
Sheffield Yorkshire, England	20 kW pulse	25	53N, 1W	20	0.3	(Density)
Lexington, Mass., United States	30 kW 50 kW pulse	36.8	42N, 71W	5	1	± 5
Stanford, Calif., United States	5 kW	30.14	37N, 122W	20	0.5	± 2.5

its range and elevation angle. The range is measured with a pulse-compression technique, in which the transmitted pulse is phase modulated with a pseudorandom code. The elevation angle is determined from a comparison of signals in two antennas with different vertical radiation patterns. Finally, the diffusion coefficient is determined from the measured amplitude decay of the trail.

The radial velocity of the target is determined from the frequency of the received signal f_r relative to the transmitted frequency f_t. When the signal is reflected from a moving target, the frequency of the received signal is Doppler shifted so that it is given by

$$f_r = \frac{1 + v/c}{1 - v/c} f_t \tag{2.1}$$

where v is the line-of-sight velocity of the moving target, positive pointing toward the station. Since the wind velocity v is much less than the speed of light, f_r can be approximated by

$$f_r = f_t + \frac{2v}{c} f_t \quad .$$

The Doppler frequency is then

$$\Delta f = f_r - f_t = \frac{2v}{c} f_t \; . \tag{2.2}$$

In the Stanford system f_r is not compared with f_t but with f_t + 40 Hz [*Nowak*, 1967]. Then the radial velocity can be determined by one measurement. If $f_r = f_t$ (i.e., for stationary targets), the output of the phase comparator will be a wave of 40 Hz. For a moving target, the Doppler frequency will be

above or below this value, depending on the sense of motion. The output of the wave comparator will give a wave frequency on the order of tens of hertz. By determining the times between the zero-crossings of the wave, Δf can be calculated. The maximum error induced in the measurement of the wind speed by this method is $\pm$ 5 m/s.

The elevation angle is an important parameter in determining the height. The more accurate the measurement of the angle, the greater is the height discrimination of the echo. In the Stanford system the signal strength of two antenna arrays are compared to determine the elevation angle [*Nowak*, 1966].

By the principle of pattern multiplication [*Kraus*, 1950], the pattern of an antenna array of identical elements is given by

$$E\ (\theta,\ \gamma) = E_e\ (\theta,\ \gamma)\ E_x\ (\theta,\ \gamma)\ E_y\ (\theta,\ \gamma)\ E_z\ (\theta,\ \gamma) \tag{2.3}$$

where

θ = zenith angle measure from the z-axis.

γ = azimuth angle measure from the x-axis.

and

E_e = pattern of a single element.

$E_{x,y,z}$ = pattern of a linear array of point sources aligned in the x, y, and z-direction, respectively.

The far field pattern of a linear array of n isotropic point sources, each spaced by a distance d is given by

$$E = E_0 \frac{\sin(n\ \psi/2)}{\sin(\psi/2)} \tag{2.4}$$

where

E_0 = field from one point source.

ψ = total phase difference of the field from adjacent sources.

$$\psi = \frac{2\pi d}{\lambda} \cos \rho + \delta \tag{2.5}$$

and

ρ = angle between the line of the array and the line from the center of the array to a far point.

δ = difference in the transmitting phase of adjacent sources.

A single-element antenna at height h above the ground can be considered an array in the z-direction. The reflection from the ground is modeled by an image source at a distance h below the ground (see Figure 2.1). Since this array is pointed in the z-direction, E_z varies only with θ. For two antennas comprised of identical elements but at different heights we get from Equation (2.3) that

$$E_1 = E_e\ (\theta, \gamma)\ E_{z1}\ (\theta)$$

$$E_2 = E_e\ (\theta, \gamma)\ E_{z2}\ (\theta) \quad .$$

The ratio of E_1 to E_2 is equal to the ratio of the signal amplitudes at the output of the two antennas.

$$\frac{S_1}{S_2} = \frac{E_{z1}(\theta)}{E_{z2}(\theta)} \quad . \tag{2.6}$$

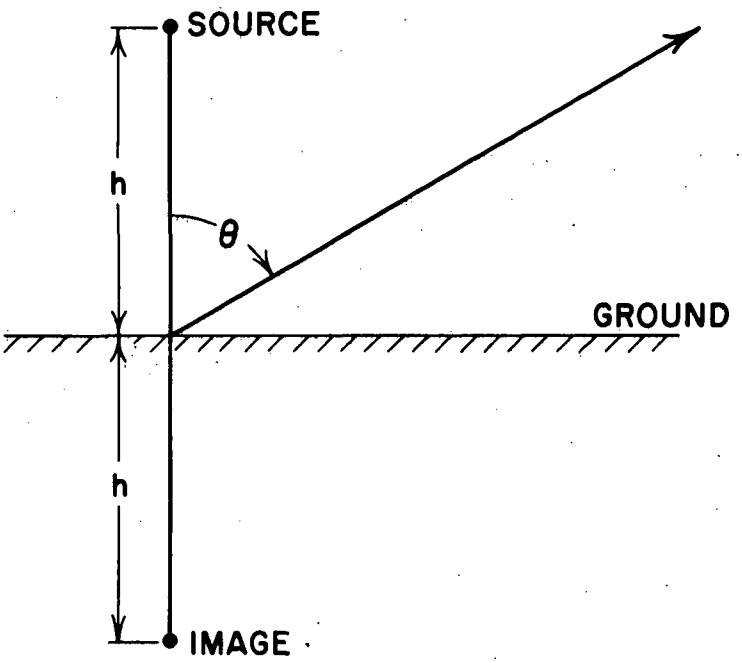

Figure 2.1 Model of reflection from the ground by an image source.

For best results, a pair of height values that leads to an amplitude ratio that varies as much as possible with θ in the area of interest is desirable. At Stanford the height values $\frac{\lambda}{2}$ and $\frac{3\lambda}{16}$ are used.

Another approach to the measurement of θ can be taken. Four point sources are located at the corners of a square whose sides are chosen in the x- and y-directions (see Figure 2.2). For the case of in-phase excitation of the array elements (i.e., $\delta = 0$), and a spacing of $d = \lambda/2$, Equation (2.5) yields for the linear array of 2 elements in the x-direction,

$$\psi_x = \pi \sin\theta \cos\gamma$$

and Equation (2.4) gives

$$E_x = E_0 \frac{\sin(\pi \sin\theta \cos\gamma)}{\sin(\pi/2 \sin\theta \cos\gamma)} .$$

Similarly, for the linear array of two elements in the y-direction

$$E_y = E_0 \frac{\sin(\pi \sin\theta \sin\gamma)}{\sin(\pi/2 \sin\theta \sin\gamma)} .$$

If antenna A_1 is now chosen as a single $\lambda/2$ dipole, the field pattern is

$$E_1 = E_{e1}(\theta, \gamma)\, E_{z1}(\theta) . \qquad (2.7)$$

If antenna A_2 is the 2 x 2 array and made up of $\lambda/2$ dipoles (so that $E_{e2} = E_{e1}$) at the same height (so that $E_{z1} = E_{z2}$), then the field pattern of A_2 is

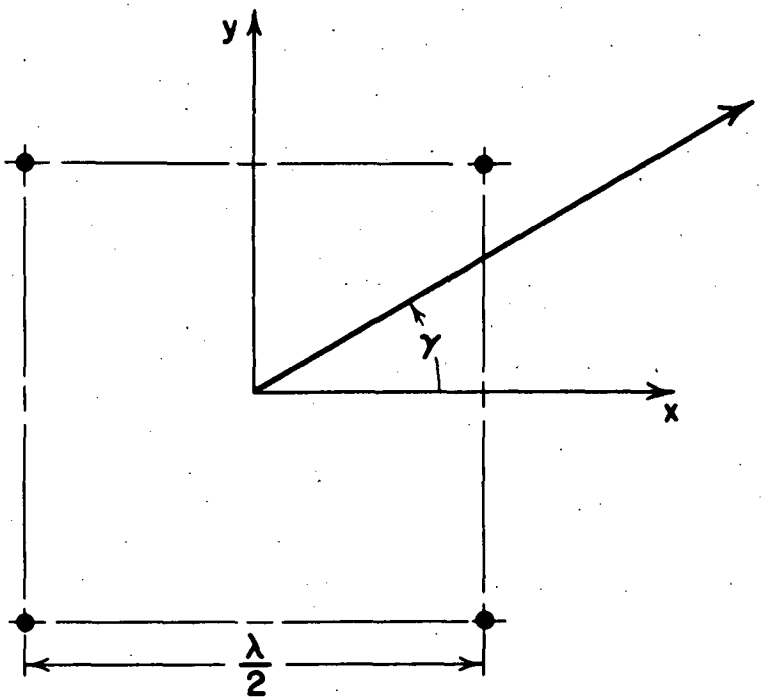

Figure 2.2 The 2 x 2 array with 4 point sources located at the corners of a square.

$$E_2 = E_{e1}\,(\theta, \gamma)\; E_{x2}\,(\theta, \gamma)\; E_{y2}\,(\theta, \gamma)\; E_{z1}\,(\theta)\,. \qquad (2.8)$$

The ratio of signal strengths is given by the ratio of Equation (2.7) to Equation (2.8).

$$\frac{S_1}{S_2} = \frac{1}{E_{x2}(\theta, \gamma)\; E_{y2}(\theta, \gamma)}\,. \qquad (2.9)$$

To make amplitude ratio vary as much as possible with θ, the two techniques described above are combined at Stanford. The signal strength of a $\lambda/2$ dipole at a height $\lambda/2$ above the ground is compared with that of a 2 x 2 array $3\lambda/16$ above the ground. Combining Equations (2.6) and (2.9) the ratio of signal strengths is

$$\frac{S_1}{S_2} = \frac{E_{z1}(\theta)}{E_{x2}(\theta, \gamma)\; E_{y2}(\theta, \gamma)\; E_{z2}(\theta)}\,. \qquad (2.10)$$

This ratio is theoretically plotted as a function of θ in Figure 2.3 [*Nowak*, 1966].

Assuming a measuring accuracy of $\pm$ 0.5 dB in the signal ratio, the maximum angle error can be determined from Figure 2.3. For elevation angle greater than 45°, an angle accuracy of $\pm$ 1° is obtainable.

To achieve high sensitivity of the system at moderate peak power, the transmitted pulse must be of fairly long duration [*Nowak*, 1967]. This fact precludes ranging with normal radar techniques, where the distance of the target is determined by measuring the time at which either the leading edge or the peak of the echo occurs. Because range accuracy is directly proportional

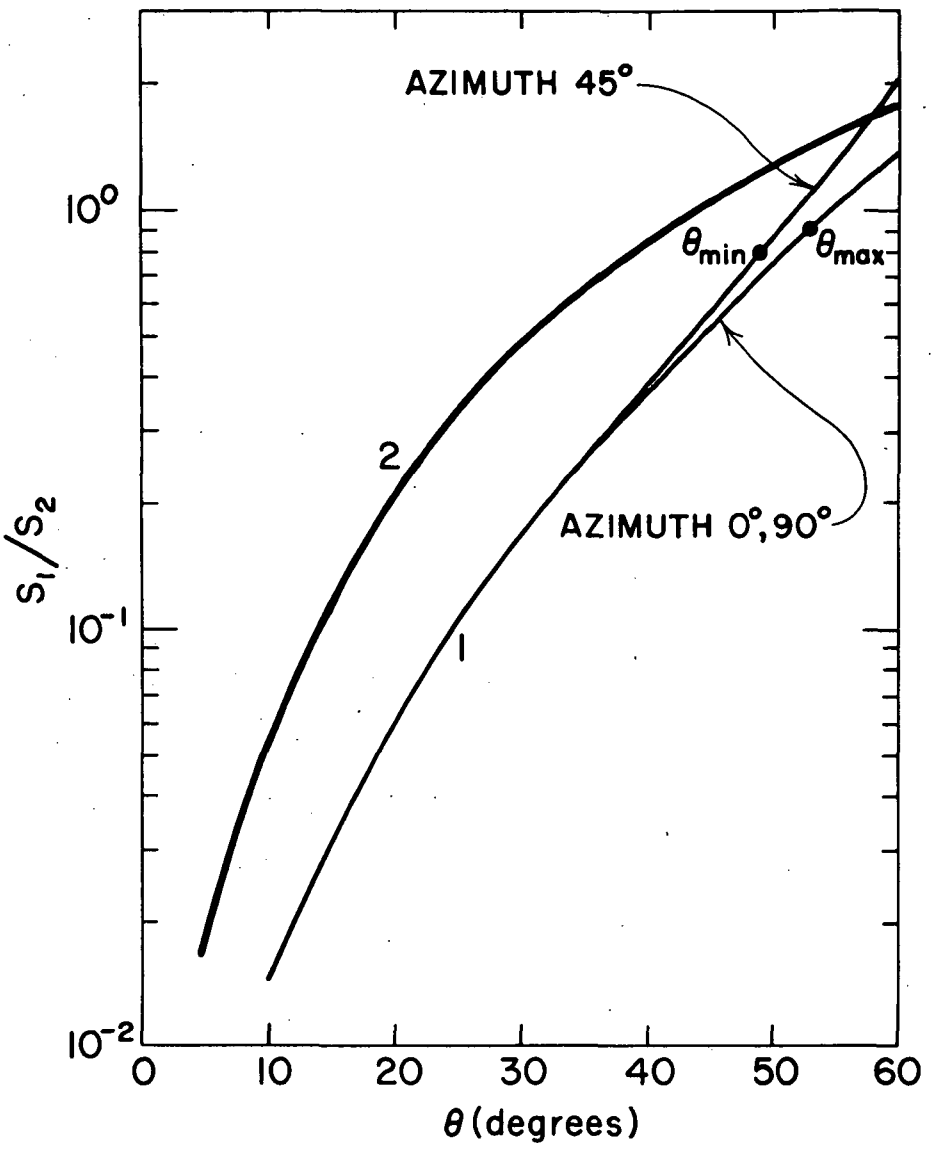

Figure 2.3 Ratio of signal strengths from two antennas, as a function of the zenith angle θ.

Curve 1. Dipole at $h_1 = \lambda/2$, 2 x 2 array at $h_2 = 3\lambda/16$ above ground

Curve 2. Identical antennas at h_1, h_2

θ_{max} and θ_{min} give the error bounds for an accuracy of $\pm$ 0.5 dB in the measurement of the pattern ratio.

to the pulse length, the long pulse employed would yield range with a completely inadequate accuracy.

In the Stanford system the range is determined by a pulse-coded technique. In this method the phase of the transmitted pulse is switched between -90° and 90° in a 28-bit code, each bit being 10 μsec in length [*Nowak*, 1967]. This pattern is recovered at the receiver and compared with the original pattern. The 28-bit code is chosen such that when the received code is correlated with the original code, a large peak amplitude occurs. This is the point at which the complete pulse has returned to the receiver. From the time at which coincidence occurs, the range of the echo is obtained as shown in Figure 2.4 [*Nowak*, 1967]. Resolution is one bit-time of the code.

Since the coded pulse consists of a coherent sequence of n subpulses of duration t_p, integrations will add signal amplitude and noise power of the individual bits, so that

$$\left(\frac{S}{N}\right)_{n \text{ pulses}} = n \left(\frac{S}{N}\right)_{\text{one pulse}} . \tag{2.11}$$

Thus, for the signal-to-noise ratio the encoded pulse of duration nt_p is equivalent to a signal pulse of length t_p with n times the peak power of the encoded pulse. The 28-bit code of the Stanford meteor radar, with a peak power of 2.5 kW is, for ranging purposes, equivalent to a 70-kW pulse of 10-μs duration.

As mentioned before, the time resolution is one bit-time of the code, or 10 μs. The resulting range resolution $\pm$ 1.5 km or, if the center of the bit is taken as reference, $\pm$ 0.75 km.

The phase-modulated pulses with their wideband spectrum (200 kHz) are unacceptable for amplitude measurements because of the very poor signal-to-

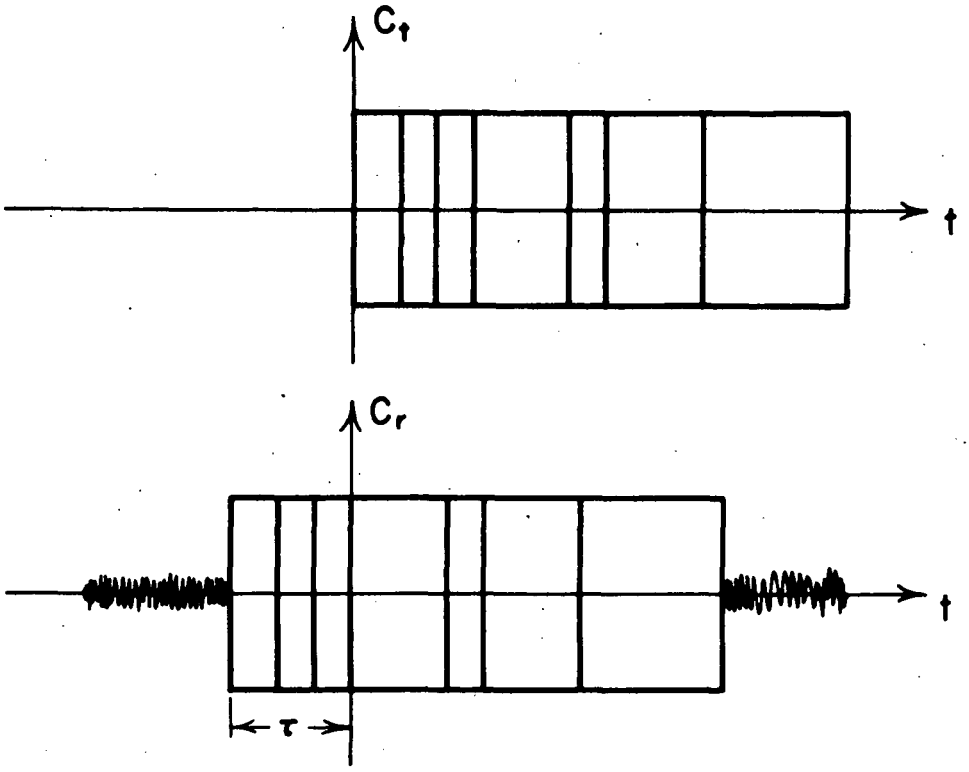

Figure 2.4 Running crosscorrelation between tramsitted and received Signals.

noise ratio associated with broadband circuits at the moderate peak power of 5 kW. An improvement of the signal-to-noise ratio similar to the ranging case is not present.

Since the measurement of the amplitude of the received signal is an indispensable part of the studies of the upper atmosphere at Stanford, a composite signal is used as shown in Figure 2.5 [*Nowak*, 1967]. Instead of changing the phase by 180° in the pulse-coded modulation (V_{11},V_{12}) as described earlier, the phase change is chosen to be 90°, leading to V_a and V_b. This modulation corresponds to adding a constant signal V_2 to the 180° phase-modulated signal V_1. Because the constant signal V_2 is a 280 μs unmodulated pulse, its bandwidth is approximately 7 kHz and the resultant signal-to-noise ratio is comparable to that used in ranging. The spectrum of the composite signal is simply the sum of the spectra of V_1 and V_2. In the region around the center frequency, almost all the power is contributed by V_2 and a narrowband filter can be used to detect it. Therefore, the signal is split into two parts, half the energy is contained in a narrowband in which the amplitude is measured and half is in a wideband for ranging.

The outputs from the receiver are digitally recorded on magnetic tape. The data are recorded essentially in raw form, and reduction of the data is left completely to a large computer.

The rate of observed meteors depend strongly on the elevation angle. At low elevation angles high data rates occur but the large range and limited accuracy of the angle measurement leads to large height errors. At high elevation angles, good height accuracies are obtained but only a few meteor trails are observed.

At Stanford this problem is attacked by splitting the measurements into

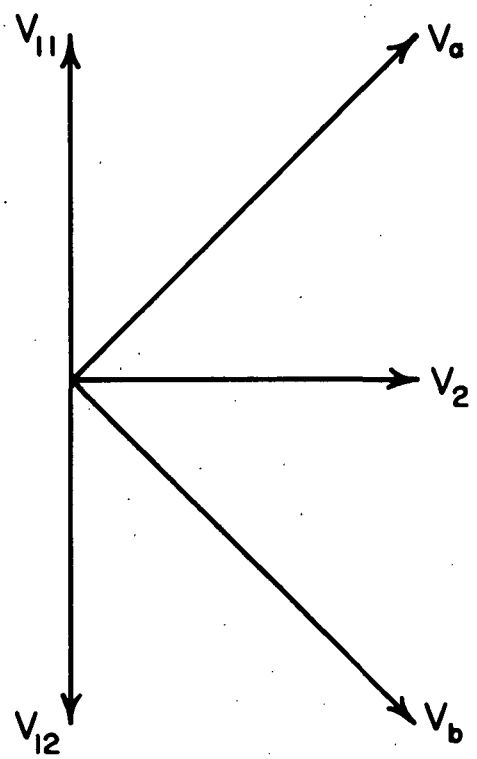

Figure 2.5 Phasor representation of the composite signal V_1 and V_2.

two parts. At high elevation angles, echo decay and height are measured only. Results show that a reasonably good correlation exists over large sampling times between decay and height, as shown in Figure 2.6 [*Nowak*, 1967]. With this established, the radial component of the wind and echo decay are measured at low elevation angles. Here range and elevation measurements are discarded. The height is determined from the echo decay by the calibration curve established earlier. Statistical analysis of the data showed standard deviations of $\pm$ 2 km or better for heights determined in this manner.

Two sets of antennas, pointing NE and NW are used to measure wind from those directions. The transmitter and the receiver are switched between the two sets of antennas at hourly intervals. A two-dimensional wind can be calculated from these measurements, but the wind needs to be time-averaged over a two-hour period.

The determination of height from a calibration curve of height vs. echo decay has been questioned. Southworth [*Deegan et al.*, 1970] has shown that echo decay does not only change with height but also is affected by the recombination of the electrons with ions in the atmosphere. Also echo decay is changed by the high wind shear that occurs (up to 100 m/s/km) in the meteor region.

In the elevation angle measurement, the simplicity of the amplitude comparison method is based on the assumption that the theoretical surve of S_1/S_2 vs. zenith angle is a good approximation to the real physical process. This assumption may be valid at Stanford, but *Frost et al.* [1970] has shown this is not the case at the University of New Hampshire. In an attempt to duplicate the amplitude comparison method for the AFCRL Meteor Radar System, it was found necessary to achieve a direct antenna calibration rather than depend

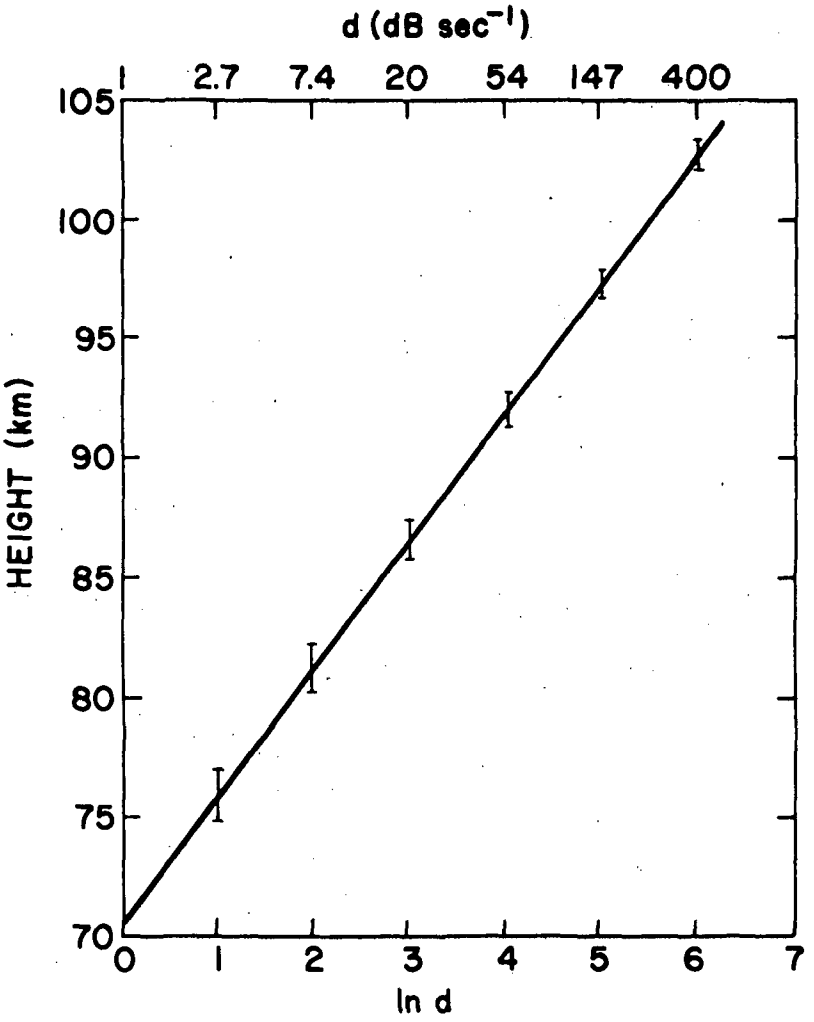

Figure 2.6 Height as estimated from echo decay d. Error bars denote 80-percent confidence.

on theoretical predictions. Because of much distortion and asymmetry in the patterns as compared to the theoretical model and of instability in the measurement, the method of angle measurement was discarded in favor of the phase comparison method [*Clark et al.*, 1970].

2.2 *AFCRL Meteor-Trails Radar*

The AFCRL System was originally located near Lexington, Massachusetts. Because of the large inaccuracies (see Table 2.1) due to excessive radio interference, the AFCRL set has been relocated at the University of New Hampshire in Durham, 80 km NNE of the original site. The transmitter has a peak power of over 30 kW and transmits at a frequency of 36.8 MHz. The techniques for measurement of the wind speed, the range and the elevation and azimuth angles are discussed here.

As in the Stanford system, the radial velocity of the wind is determined from the Doppler shift of the returned signal. In the AFCRL system two measurements are made of Δf using the transmitting frequency f_t as one reference and f_t + 25.6 MHz as another reference. The value of the offset was selected to correspond to a trail drift velocity of 100 m/sec. An echo with low wind speed will show about a 25 Hz difference in frequency with respect to this offset reference. In practice Δf is measured by determining the time within one Doppler cycle. The error inherent in this measurement is $\pm$ 5 m/s.

The range is determined by measuring the time delay between the transmitted pulse and the received pulse. A 124-kHz clock is used for the measurement. The system considers only those range counts, or timing pulses, which fall in the interval $\pm$ 2 counts of the count obtained that fall outside the interval.

The period of the 124 kHz clock is 8.06 μs. Since the timing of the returning pulse is limited by this time period, this is the maximum error in range associated with each pulse. The range error is then ± 1.2 km. If a large number N of pulses is taken, the error is divided by $\sqrt{N}$. In the AFCRL system, the usual number of pulses is 50, so that the error is about ± 0.2 km.

In an attempt to use the amplitude comparison method to determine the elevation angle, the AFCRL engineers found a great deal of difficulties in calibrating the antenna arrays to determine the relationship between amplitude ratio and elevation angle. From the observations made during 1969, approximate calibration contours were made for the antenna arrays [*Frost and Clark*, 1970]. Examinations of these results and earlier preliminary estimates of theoretical patterns led to the following conclusions. There was considerable distortion and asymmetry in the patterns as compared to the theoretical model. This was due to the limited extent of the ground plane to coupling between the various antenna arrays, and to the proximity of the radar instrument van. Also, due to reasons that could not be identified, the patterns were not stable and significant changes were noted between initial observations made in April 1969, and later ones made in November 1969.

As a consequence a study was made in the Fall of 1969 leading to the use of a phase comparison interferometer for elevation angle measurements. This technique used the phase difference between two adjacent antennas to determine the direction of arrival of a reflected pulse, as shown in Figure 2.7. The wavefronts of the return wave arrives at one antenna before the other. The amount of delay or the phase difference is due to the difference in path length Δl. Since $\Delta l = d \cos \beta$, the phase difference is

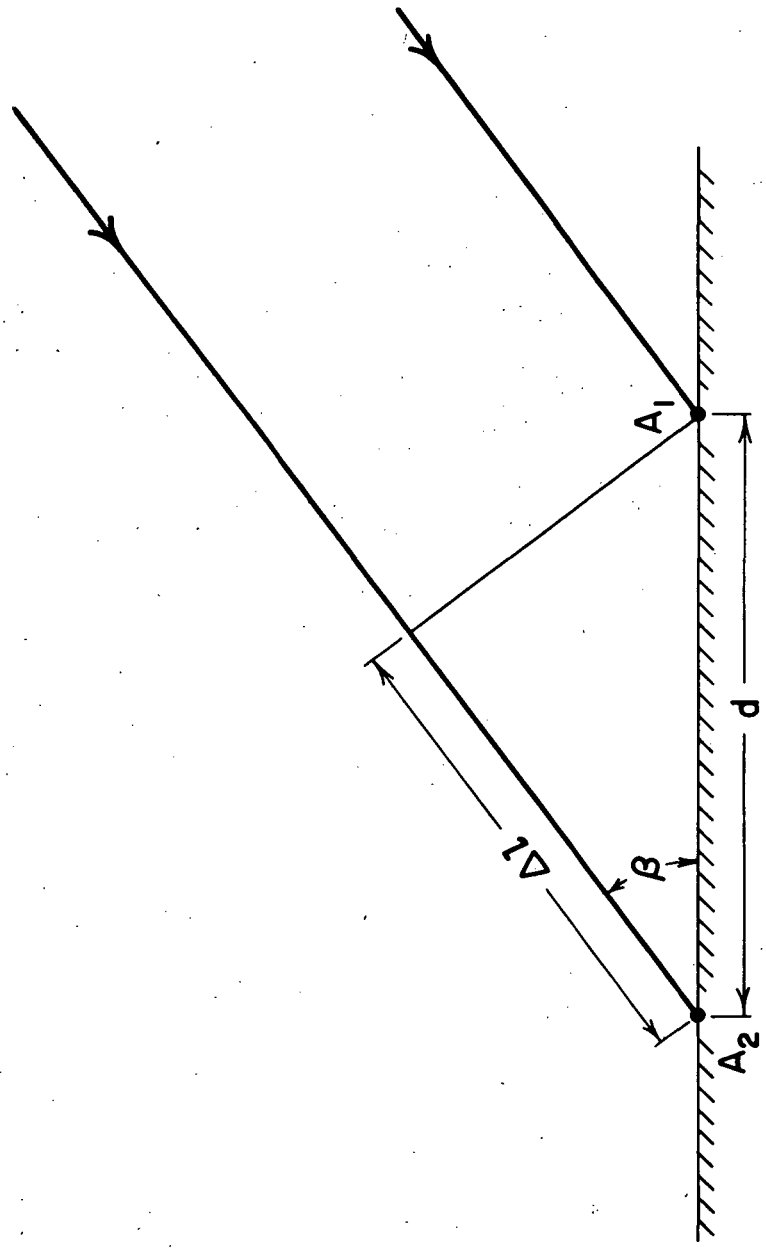

Figure 2.7 Difference in ray-path lengths to two spaced antennas.

$$\Phi = \frac{2\pi d}{\lambda} \cos \beta \tag{2.12}$$

where

d = distance between the antennas

λ = wavelength of the transmitted signal

β = angle between the line of the two antennas and the line from one of the antennas to a reflection point on the trail.

For an arbitrary location of the target the angle β is a function both the elevation angle and the azimuth angle.

At the University of New Hampshire, the phase difference is measured directly with a phase comparator. The output voltage $v(\beta)$ of the phase comparator [*Clark et al.*, 1970] is

$$v(\beta) = k \sin(\phi_\tau + \frac{2\pi d}{\lambda} \cos \beta) \tag{2.13}$$

where k is a constant proportional to the amplitude of the received signal. Figure 2.8 shows a plot of $v(\beta)$ for $\phi_\tau = 0$ and $d = 1.5\lambda$. ϕ_τ is a variable artificial phase shift introduced into one of the receivers. This variable phase shift is used to move a null of the pattern of $v(\beta)$ through a target. When this occurs, the angular position of the target is known. ϕ_τ is varied from 0 to 180° in 10 discrete steps in the AFCRL system.

As seen in Figure 2.8 [*Clark et al.*, 1970], the sector of interest is within lobes 3 and 4. This is due to the fact that adjacent lobes are distinguishable by polarity, but beyond adjacent lobes ambiguity occurs. That is, a target in the direction of lobe 3 is a distinguishable from one in the direction of lobes 2 or 4, but targets from lobes 2 and 4 are indistinguish-

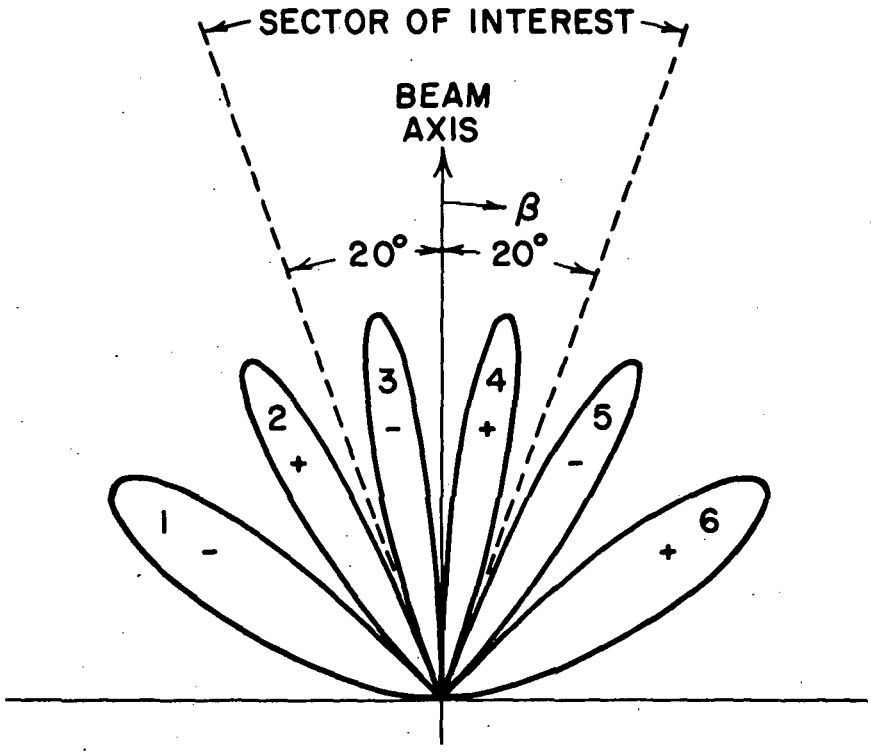

Figure 2.8 A plot of the output of the phase comparator $v(\beta)$.

able from each other. Radar returns are ensured of being detected only within the sector of interest by keeping the gains of antennas high within the sector and low outside the sector.

To measure the azimuth angle, a third antenna A_3 is used in conjunction with one of the elevation antennas to provide an interferometric baseline which is perpendicular to the elevation baseline. Since the signal processing needed is identical to that needed for the elevation signal, the same equipment is time shared. The elevation accuracy is $\pm$ 1.5° and the azimuth accuracy is $\pm$ 1°.

Return pulses from an individual meteor trail first impinge on the antennas and travel to the receivers. The ouput amplitudes and signs are stored on magnetic tape. The magnetic tape then is processed off-line on a high speed digital computer to determine the wind speed and height of the trails.

To determine the two-dimensional wind, the AFCRL system used two arrays of antennas, one pointing NE and another NW, for alternate periods of time. All the antennas are inclined 45° above the ground plane.

2.3 *The French Continuous-Wave Radar*

In France a continuous-wave bistatic radar was built in which the Doppler shift, the distance, and the direction of arrival are all obtained by means of phase comparisons [*Spizzichino et al.*, 1965]. The transmitter located at Garchy delivers continuous waves at a frequency of 29.792 MHz and has a peak power output of 5 kW. The receiving station is at Sens-Beaujeu, 20 miles west of Garchy. The direct wave necessary for phase comparison is received from the transmitter by means of a vertically polarized antenna.

Like the other meteor radar systems, the wind speed is determined from the Doppler shift of the received signal. By means of a phase comparator,

the phase difference $\Delta\phi$ between the reflected wave and the wave directly transmitted through the vertically polarized link is measured and, as a result, the Doppler shift is easily determined.

The phase comparator yields two outputs which are proportional to the sine and the cosine of the phase difference $\Delta\phi$. The sense of the drift is determined by the relative phase progression of the two waves. For example, if the sine wave is leading the cosine wave, the meteor is approaching the radar. The accuracy of the radial velocity measurement is 1 m/s for a SNR of 20 dB.

As in the AFCRL system, the receiving station at Sens-Beaujeu has three receiving antennas located in the vertices of a right triangle with one of the sides parallel to the beam axis, to measure both the elevation and the azimuth angles. The phase difference Φ_1 between the fields received by the two antennas parallel to the beam axis is measured (see Figure 2.7). The outputs of the phase comparator are two voltages, $e \cos \Phi_1$ and $e \sin \Phi_1$. They are applied to the plates of an oscillograph, producing a polar diagram of e and Φ from which the phase Φ_1 can be determined directly. For the two antennas perpendicular to the beam axis, the phase difference Φ_2 is also determined. From Φ_1 and Φ_2 the elevation angle and the azimuth angle are computed.

An angle accuracy of $\pm$ 0.2° for a SNR of 25 dB has been claimed for the French system. This precision has been questioned since it is extremely difficult to find a calibration standard with the accuracy of 0.1°, and this is the very minimum required to check an error limit of 0.2° of the angle measurement [*Nowak*, 1970].

The phase comparison method is again used to measure the range. Two waves with frequencies f_1 and f_2 are transmitted simultaneously. If the waves are

reflected off a trail at a distance R from the radar, the received fields are proportional to

$$E_1 = \exp i(2\pi f_1 t + \frac{4\pi}{c} f_1 R)$$

$$E_2 = \exp i(2\pi f_2 t + \frac{4\pi}{c} f_2 R) \quad .$$

The same transmitted waves are also received directly through the vertically polarized link after traveling the distance R_0 separating the transmitting and receiving stations. They are represented by

$$E_1' = \exp i(2\pi f_1 t + \frac{2\pi}{c} f_1 R_0)$$

$$E_2' = \exp i(2\pi f_2 t + \frac{2\pi}{c} f_2 R_0) \quad .$$

After mixing E_1' and E_2', a component proportional to

$$E_1'' = \exp i[2\pi(f_2 - f_1)t + \frac{2\pi}{c} R_0(f_2 - f_1)]$$

is filtered out. This is, in turn, mixed with the field E_1 to yield, after filtering, a component proportional to

$$E_1''' = \exp i[2\pi f_2 t + \frac{2\pi}{c} (f_2 R_0 - f_1 R_0 + 2f_1 R)] \quad .$$

Two waves E_1''' and E_2 are obtained with the same frequency f_2 whose phase difference is measured with the same equipment as that used for angle measurement.

The phase difference

$$\Delta\phi_{12} = \frac{2\pi}{c} (f_1 - f_1) (2R - R_0) \tag{2.14}$$

then yields the range R.

The difference between the frequencies f_1 and f_2 is made small so that the phase difference $\Delta\phi_{12}$ given by Equation (2.14) varies by no more than 2π. With the error in $\Delta\phi$ known, the range R can be determined to within 2 km. To improve the accuracy, a third wave with the frequency f_3 is used such that the difference $(f_1 - f_3)$ is much larger than $(f_1 - f_2)$. Operating on f_1 and f_3 in the same way as on f_1 and f_2, the phase difference $\Delta\phi_{13}$ is obtained which give a much more accurate, but ambiguous, value for R. The ambiguity is resolved by measuring $\Delta\phi_{12}$. The measurement of $\Delta\phi_{13}$ thus plays the role of a vernier. By measuring both $\Delta\phi_{12}$ and $\Delta\phi_{13}$, the range error is reduced to 300 meters for a SNR of 20 dB.

At Sens-Beaujeu an array of antennas are pointed east and 45° above the ground plane, to measure the east-west component of the wind. Recently, a transmitter and another antenna array was built at Bar-su-Aube that points south, to measure the north-south component of the wind [*Glass et al.*, 1970]. This set covers the same area of the sky as the eastward pointing array. Thus, it is possible to measure both components of the horizontal wind simultaneously.

The meteor trails observations made in Garchy clearly confirms the existence of the various components of the measured winds-prevailing wind, tides, gravity waves. The observations suggest that these components are strongly interacting. A theoretical study of non-linear effects has been carried out to study these interactions [*Spizzichino*, 1969a, 1969b, 1969c, 1969d, 1970a,

1970b]. It suggests in particular that the diurnal tide yields energy to gravity waves propagating through the mesosphere. Such a mechanism is said to be consistent with many observed properties of tides and gravity waves.

2.4 *Adelaide Radio-Meteor System*

At Adelaide, South Australia, measurements of the motion of the upper atmosphere by radio observations of drifting meteor trails began in 1952 using a combined continuous wave and pulse technique. The present system consists of two transmitters, continuous wave and pulse, at Adelaide, a main receiving station at St. Kilda, and three outstations [*Barnes and Pazniokas*, 1968]. Data from the outstations are relayed by FM links to the main station where all the information is recorded. The CW transmitter is used to measure the line-of-sight velocity of the meteor trails and the angle of arrival of the reflected waves. The pulse transmitter is used to measure the range of the reflected echoes.

The drift of the meteor trail is obtained at the receiving antenna by comparing the phase of the sky wave reflected from a meteor trail with the phase of the ground wave received directly from the transmitter. This method of Doppler measurement is very similar to that used in the French Meteor Radar System. The instrumental accuracy for wind speed determinations is $\pm$ 5 m/s.

The sense of the drift is determined by a periodic saw-tooth phase modulation of the transmitted wave. The phase is retarded by 90° every 20 ms. Because of the path differences, the 90° phase retardation of the sky wave occurs 0.5 to 1 ms after that of the ground wave. That is, during this period the ground wave *G* is retarded in phase by 90° but the phase of the sky wave *S* is changed, as shown in Figure 2.9 [*Barnes and Pazniokas*, 1968]. For this interval the vector triangle GSR is replaced by G'S R' and the resultant ampli-

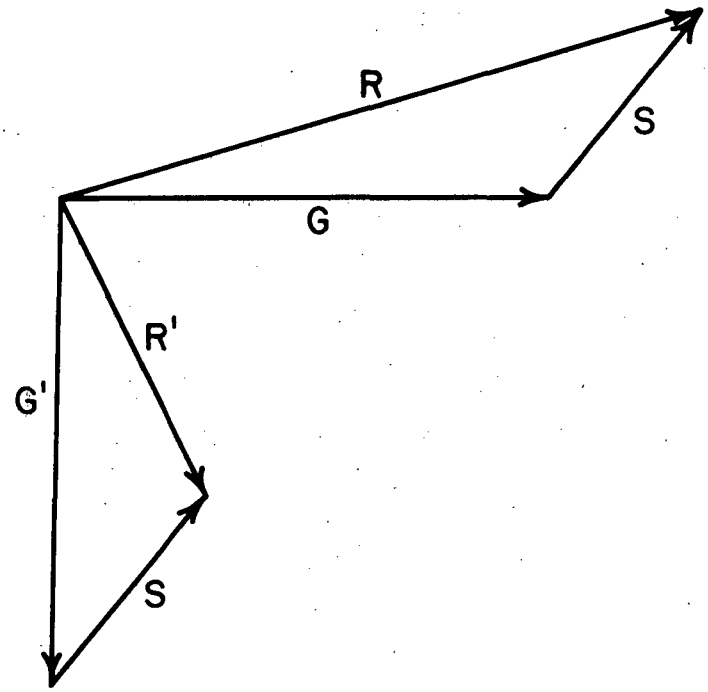

Figure 2.9 Phase diagram showing the resultant amplitude at the receiving antennas in terms of the ground wave G and the sky wave S.

tude at the receiver changes from R to R'. On the Doppler record the amplitude R' appears as spikes which delineate a phantom trace. The sense of the drift of the meteor trail is obtained by determining whether the phantom trace leads or lags the main Doppler wave.

The angle of arrival of the reflected wave is found by a comparison of the phases of the sky wave at five-spaced receiving antennas at the main station. The layout of the antenna system is shown in Figure 2.10 [*Barnes and Pazniokas*, 1968]. The directions OE and ON define the positive axes of a cartesian coordinate system. The sky wave is defined with respect to this coordinate system by the direction cosines l and m. The transmitter lies on the line OS. By comparing the phases of the Doppler signals at the antennas, the elevation and the azimuth angles are determined unambiguously. Errors in the determination of the angle of arrival are less than $\pm$ 1°.

The range of the meteor trail with respect to the receiving site is determined by measuring the time difference between the arrival of a ground wave pulse and the associated sky wave pulse and making an appropriate correction for the separation of the transmitting and receiving sites. The equipment parameters permit a range accuracy of $\pm$ 200 meters.

The diurnal, seasonal, and height variations of the wind are obtained by setting up a model of the variation of the zonal, meriodional, and vertical components as a function of time and height and determining the parameters of the model by comparison with the observed data. The computer analyses are carried out according to a method developed by *Groves* [1959].

2.5 *Sheffield Meteor Wind Experiment*

The radar system used in the Sheffield Meteor Wind Experiment is a coherent pulse type similar to the one used by *Greenhow* [1964]. The transmitter

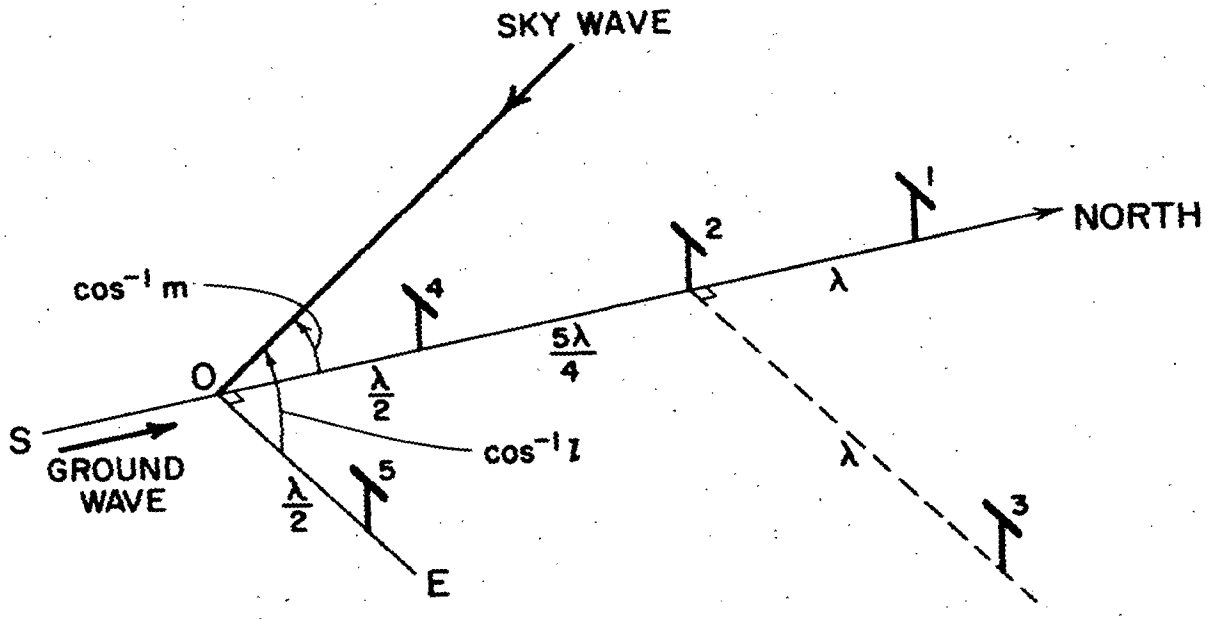

Figure 2.10 Layout of the antennas used for determining the direction of arrival of the sky wave.

provides a peak power of 200 kW at a frequency of 36 MHz.

In recent years special efforts have been made at Sheffield to develop equipment for the resolution of the vertical structure of the horizontal wind in the 80 to 110 km region [*Muller*, 1970]. The system that evolved is capable of resolving the position of the specular reflection point on a meteor trail in terms of elevation angle, azimuth angle and range as well as the radial velocity.

Like other meteor radar systems, the radial velocity of the target is measured from the Doppler shift. The outputs of the phase comparator are two waves whose amplitudes are proportional to the sine and cosine of the phase difference between the transmitted signal and the associated received signal. The Doppler frequency is determined directly from the spacing of the amplitude zeros. The sense of the drift is indicated by the relative phase progression of the two waves. For the case where the sine wave is leading the cosine wave, the meteor is approaching the radar. The wind speed accuracy is $\pm$ 2 m/s.

The range of the target is obtained from the time interval between the transmission of a pulse and its return after reflection from a meteor trail. Every other pulse is doubled in length to facilitate this measurement.

The elevation angle and the azimuth are measured by a phase comparison method similar to that used at the University of New Hampshire. The measurement of the angles depend on the determination of the phase differences between three points of a right triangle on the ground.

Three antenna arrays pointing NW, NE and SW are used to determine the two components of the horizontal wind. The arrays in the NW and NE directions are intended for routine wind studies. The SW array is intended for special

investigations involving remote stations, which are more conveniently built SW of the main station.

A multi-station phase-coherent experiment is being developed at Sheffield to study the vertical structure of the horizontal wind in the meteor zone by measuring up to three reflection points on the same meteor trail. The two receiving sites secured for this experiment are located at Ughill, 4.5 km SW of the main station, and at Tideslow, 19.5 km SW along the same azimuth. The experiment relies upon the reception of the meteor echo at the two receiving sites and re-transmitting it to the main station so that the radial velocity components from each site can be determined. Each remote station is controlled remotely by a VHF command signal and the meteor echo information is relayed to the main station through a high frequency link.

2.6 *Havana Meteor Radar Network*

The Havana system was an eight-station multistatic phase-coherent network. The original six sites, which included the main station and five outlying stations, were obtained from the Harvard Radio Meteor Project [*Hawkins*, 1963]. Two remote sites were added for wind studies. At the main site, a pulse transmitter delivered a peak power of 3 Mw at a frequency of 40.92 MHz. Also at the main site, a dual-channel receiver provided Doppler information, range, angle of arrival, and Fresnel pattern. At each one of the outlying receiving sites, a single-channel receiver provided information concerning Doppler shift, range and Fresnel patterns. Work at Havana has been discontinued and much of the equipment is now being used to construct the new facility at the University of Illinois.

Echoes were received at the main site if the meteor trail was tangent to a sphere whose center was at the main site and whose radius was the distance

from the site to the trail. An echo was also received at an outlying site if the trail was tangent to an ellipsoid whose foci were the receiving site under consideration and the main site. The measured Doppler frequency at one of these sites provided the velocity wind component perpendicular to the ellipsoid at the point of tangency.

The output of the phase comparator were two waves that had amplitudes proportional to the sine and cosine of the phase change in a similar manner as was done at the French and Sheffield systems. The sense of the drift was determined from the relative phase progression of the two waves. A least-square curve-fitting process was applied to the phase information giving a radial velocity determined to an accuracy of $\pm$ 1 m/s.

The range was determined from the number of quarter microseconds between the transmission and reception of a pulse at a receiving site. Every 5th pulse transmitted was delayed by 8 μsec to facilitate the measurement. The error was $\pm$ 150 meters.

To locate the position of the meteor trail, the gradient of the direction of the meteor in space was determined by finding the times between reflection points [*Deegan et al.*, 1970]. The double-trough antenna located at the main site was used to supplement the location of the trail. The two sections of the antenna were arranged to be used as an interferometer. At every echo reception a cone of possible meteor locations was identified in the reduction procedure, which provided additional intersecting surfaces for target positioning. The height resolution was limited by the difficulty in determining the velocity of the meteoroid [*Barnes and Pazniokas*, 1968]. The height accuracy was $\pm$ 3 km.

To determine the two horizontal components of the wind, two line-of-sight velocities had to be obtained simultaneously from a remote site and at one of the six original stations. A three-dimensional wind determination required that echoes from a trail be received simultaneously at a remote site and two outlying sites which were distant from each other.

The detail with which the wind field could be described depended upon the meteor influx rate, which was high from shortly after midnight to midafternoon. During this part of the day, the average rate of meteors from which horizontal wind could be determined was about 250 per hour.

All the data collected by the eight stations were sent to the main site for processing in a digitizer and recording in a multichannel digital tape recorder. The tape was played back in a CDC-6400 computer appropriately programmed to print out wind profiles.

The Havana system was noted for its complexity and high costs (see Table 2.1). The receiving system contained a complicated configuration of delay lines and eight echo-pattern recognizers. The cost to reproduce the Havana system would be over $2,000,000, five times more than the cost of any other meteor radar system.

In summary, radar meteor trail returns can provide wind information between 80 and 120 km during the day as well as at night, during foul weather as well as fair. A sufficient number of stations now exist to begin large-scale synoptic and tidal wind studies north of 30 N. However, cooperation among these stations so as to coordinate their observations is needed to do so.

3. ECHOES FROM METEOR TRAILS

3.1 *Introduction*

Each day billions of meteors enter the earth's atmosphere and, in burning, form long columns of ionized particles. These columns diffuse rapidly and usually disappear within a few seconds. But during their brief existence the ionized columns will reflect radio signals, thus giving a rise to what is called meteor scatter. Its most important use has been in upper atmosphere research. It is also one of the principal ways in which the meteors themselves are studied.

Since 1946 the physical processes involved in the interaction of meteors with the upper atmosphere have been studied extensively. Several hundred papers have been published on the subject. Much of this work is summarized in a book by *McKinley* [1961]. It is the plan of this chapter to do a survey of those characteristics of meteors and meteor ionization which are important to the understanding of radar returns from meteor trails. The subject matter to be discussed will deal with those characteristics of meteoric particles and meteor trails which are pertinent to their radio reflection properties. Then, these properties themselves, as observed for individual trails, are discussed.

3.2 *Meteoric Particles*

The meteors of interest are those particles entering the earth's atmosphere that are completely burned up by frictional heating. There are the smaller particles, the micrometeorites, which slowly settle through the atmosphere without being destroyed. Also, there are large meteors which manifest themselves as fireballs and even larger ones which reach the earth's surface

as meteorites. The micrometeorites are not of concern because, even though they are most numerous, they enter the earth's atmosphere too slowly to produce any significant ionization. The large meteoroids, even though they produce substantial ionization, are of little concern here because their rate of occurrence is extremely low.

Some of the properties of meteoric particles are summarized in Table 3.1 [*Sugar*, 1964]. The particles of interest in meteor scatter are those with masses in the range 10^{3} to 10^{-7} gram. Before being trapped by the gravitational field of the earth, these particles move in orbits around the sun. Their composition is uncertain; however, they appear to be of cometary origin [*McKinley*, 1961]. A substantial fraction of them are not single particles but fragile loosely-found agglomerates, sometimes called "dustballs".

Meteors can be divided into two classes, the shower meteors and the sporadic meteors. The shower meteors are a collection of particles all moving at the same velocity in fairly well-defined orbits or streams around the sun. Their orbits intersect the orbit of the earth at a specific time each year and at these times meteor showers are observed. These meteors, while the most spectacular, account for only a small fraction of all meteors. It is the sporadic meteors that are of most interest in upper atmospheric research. Sporadic meteors are those which do not have well-defined streams but rather seem to move in random orbits. Therefore, whereas shower meteors appear to be coming from a specific point in the sky--the radiant point for the shower--sporadic meteors have radiants that appear to be randomly distributed over the sky.

Shower meteors are most easily recognized in terms of their radiants, velocities, and time of occurrence, since these parameters are relatively fixed.

TABLE 3.1

Order of magnitude estimates of the properties of sporadic meteors.

	Mass (grams)	Visual Magnitude	Radius	Number of this mass or greater swept up by the earth each day	Electron line density (electrons) per meter of trail length)
Particles pass through the atmosphere and fall to the ground	10^{4}	-12.5	8 cm	10	-
Particles totally disintegrated in the upper atmosphere	10^{3}	-10.0	4 cm	10^{2}	-
	10^{2}	-7.5	2 cm	10^{3}	-
	10	-5.0	0.8 cm	10^{4}	10^{18}
	1	-2.5	0.4 cm	10^{5}	10^{17}
	10^{-1}	0	0.2 cm	10^{6}	10^{16}
	10^{-2}	2.5	0.08 cm	10^{7}	10^{15}
	10^{-3}	5.0	0.04 cm	10^{8}	10^{14}
	10^{-4}	7.5	0.02 cm	10^{9}	10^{13}
	10^{-5}	10.0	80 microns	10^{10}	10^{12}
	10^{-6}	12.5	40 microns	10^{11}	10^{11}
	10^{-7}	15.0	20 microns	10^{12}	10^{10}
	10^{-8}	17.5	8 microns	?	?
Micro-meteorites (Particles float down unchanged by atmospheric collisions)	10^{-9}	20.0	4 microns	Total for this group estimated as high as 10^{20}	Practically None
	10^{-10}	22.5	2 microns		
	10^{-11}	25.0	0.8 micron		
	10^{-12}	27.5	0.4 micron		
Particles removed from the solar system by radiation pressure	10^{-13}	30	0.2 micron	-	-

The radiants and times of occurrence of sporadic meteors are random and thus cannot be cataloged in any specific manner. Their radiant points are not, however, uniformly distributed in the sky but are mostly concentrated toward the ecliptic plane--the plane of the earth's orbit--and move in the same direction around the sun as does the earth [*Hawkins*, 1956]. The orbits are not uniformly distributed along the earth's orbit but are concentrated so as to produce a maximum incidence of meteors on the earth in July and a minimum in February. This variation in space density of meteors is shown in Figure 3.1 [*Sugar*, 1964].

The rate of incidence of sporadic meteors on the earth is further modified by two factors. The first of these, which results in a regular diurnal variation in meteor rate, is illustrated in Figure 3.2. On the morning side of the earth, meteors are swept up by the forward motion of the earth in its motion around the sun. On the evening side the only meteors reaching the earth are those which overtake it. This results in a maximum occurrence rate around 6 a.m. and a minimum rate at 6 p.m. It has been shown that for a radar located in the northern hemisphere and elevated at 45° the maximum rate of occurrence of meteors is north at 6 a.m., east at 12 noon, south at 6 p.m., and west at 12 midnight [*Villard et al.*, 1955]. The other factor affecting the rate incidence of sporadic meteors is the tilt of the earth's axis relative to the ecliptic plane. This gives rise to a seasonal variation that is dependent on the latitude of the observer and can change the expected hourly rates by a factor of 1.4.

The velocities of meteors approaching the earth are in the range 11.3 to 72 km/sec. The lower limit is the escape velocity of a particle leaving the earth's gravitational field and therefore is the lowest velocity that a parti-

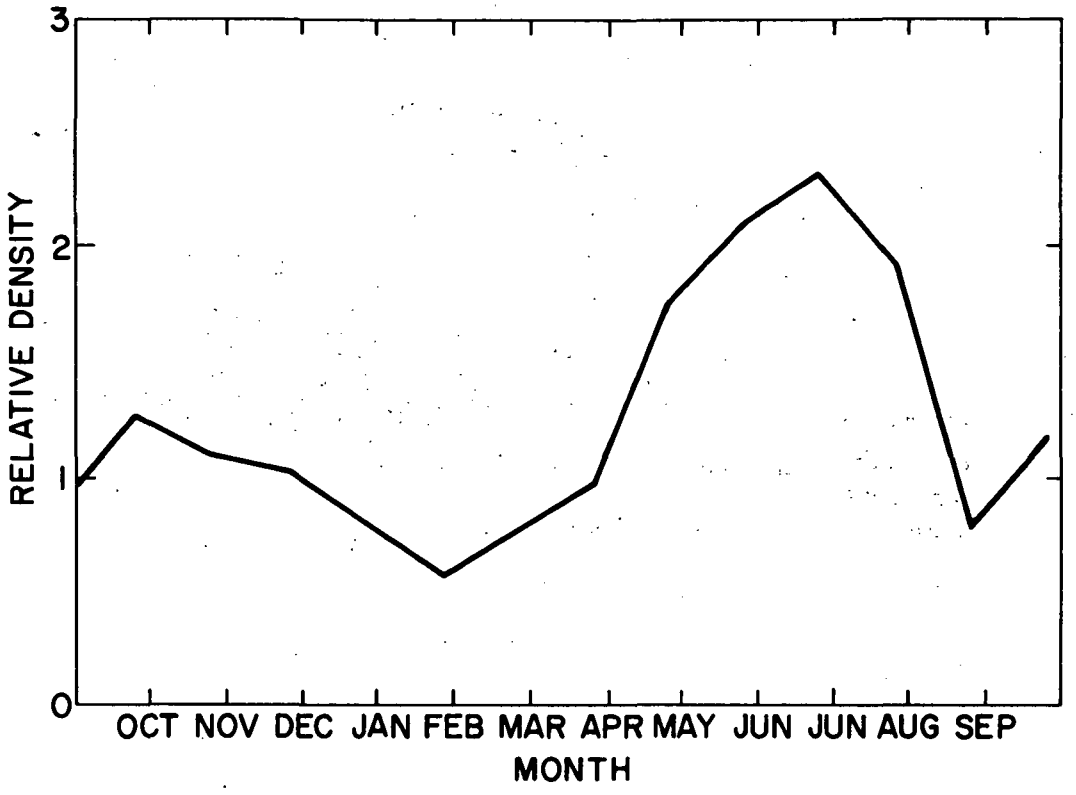

Figure 3.1 Variation in the space density of meteors along the earth's orbit.

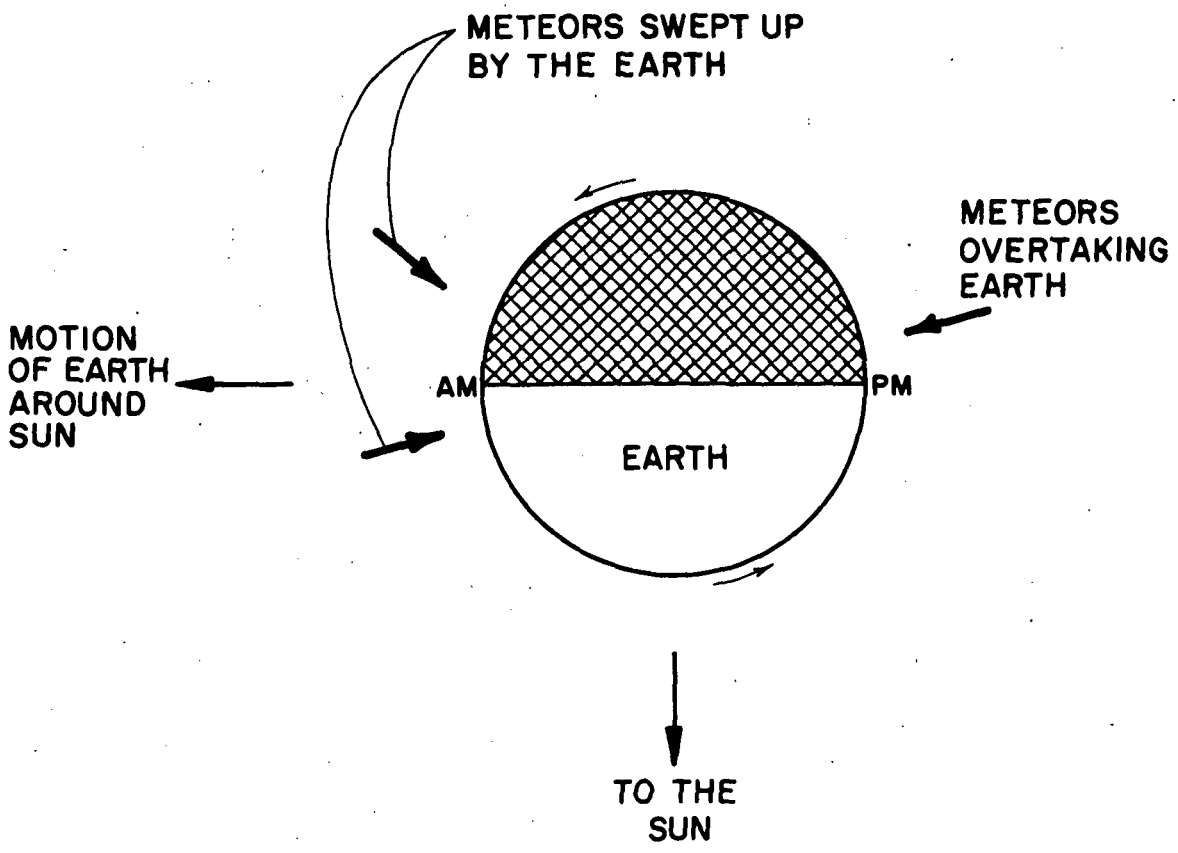

Figure 3.2 Diurnal variation of meteor rates.

cle falling toward the earth can have. The upper limit is the sum of two components, a 30 km/sec component associated with the velocity of the earth in its orbit around the sun, and a 42 km/sec component which is the escape velocity for a particle leaving the solar system. Nearly all observations have indicated that meteor velocities fall in the above range and that the meteors are thus members of the solar system.

3.3 *Meteor Trails*

As a meteoric particle enters the earth's atmosphere, it collides with air molecules. The impact energy produces heat which evaporates atoms from the meteor, and these atoms move off with a velocity which is substantially equal to that of the meteor. Collisions between these high velocity atoms and the surrounding air result in the production of heat, light and ionization, which is distributed in the form of a long, thin, paraboloid of revolution with the particles at the head of it. The electron line density of the trail is proportional to the mass of the particle. No appreciable ionization is formed until the particle enters the relatively dense air at heights below 120 km. Above this height collisions of the particles with air molecules are not frequent enough to form a trail. As the particle traverses the region below 120 km it vaporizes rapidly, and most particles are completely evaporated before reaching 80 km. The relatively small thickness of the meteor region is a result of the rapid change in air density which occurs over the height range quoted. At 120 km the mean free path is 5.4 m and this decreases to 3.8 mm at 80 km [*Sugar*, 1964].

The height distribution of meteor trails varies with the velocity, mass and radiant of the meteor. The higher velocity particles produce trails at the higher heights as is shown in Figure 3.3 [*McKinley*, 1961]. The particle

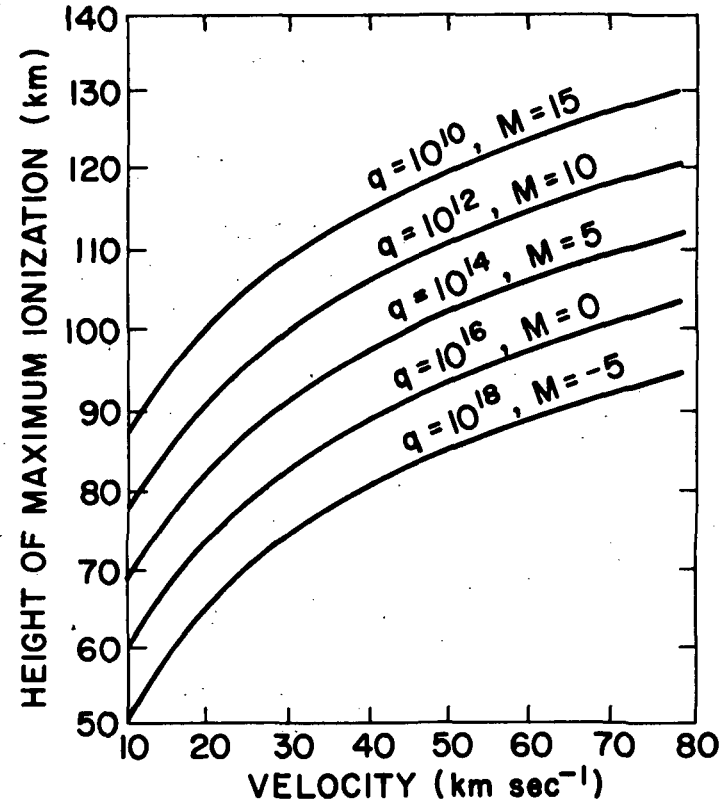

Figure 3.3 Height of point of maximum ionization as a function of velocity.

of higher mass produce maximum trail ionization at lower heights. A variation in the meteor mass from 10^{-7} to 10 g gives a height variation in the trail occurrence of approximately 35 km. Also, trails with greater zenith angles reach their ionization maximum at greater heights. A typical distribution of numbers versus height is shown in Figure 3.4, based on 548 meteor observations made at Ottawa [*McKinley*, 1961].

The length of meteor trails--the length of path over which the ionization exceeds an arbitrary threshold electron line density--is dependent on the particle mass, velocity and zenith angle. The brighter and faster meteors create longer trails, as do meteors arriving from radiants near the horizon. For an electron line density of 10^{12} elec/m the average trail length is 25 km [*Eshleman*, 1957].

The initial trail radius is typically 0.55 m at a height of 80 km and 4.35 m at 120 km. Once the trail is formed it expands by diffusion at a relatively low rate, producing a radial distribution of material that is approximately Gaussian. The quantity $(4\ Dt + r_0^2)^{1/2}$ may be taken as the approximate radius of the trail after a time t where D is the diffusion coefficient and r_0 is the initial radius of the trail [*Sugar*, 1964]. D varies from 0.3 m^2/sec at 80 km height to 167 m^2/sec at 115 km [*Nowak*, 1967]. Thus, after one second a trail will have a radius in the range 1.2 to 26 m.

The practical lifetime of an observed trail is, of course, dependent on the means for detecting it. Most trails detected by radio means are those resulting from small particles and thus last only a fraction of a second.

3.4 *Reflection Properties of Individual Trails*

Meteor trails can be divided into two classes, underdense trail and overdense trails. Underdense trails are those where the electron density is low

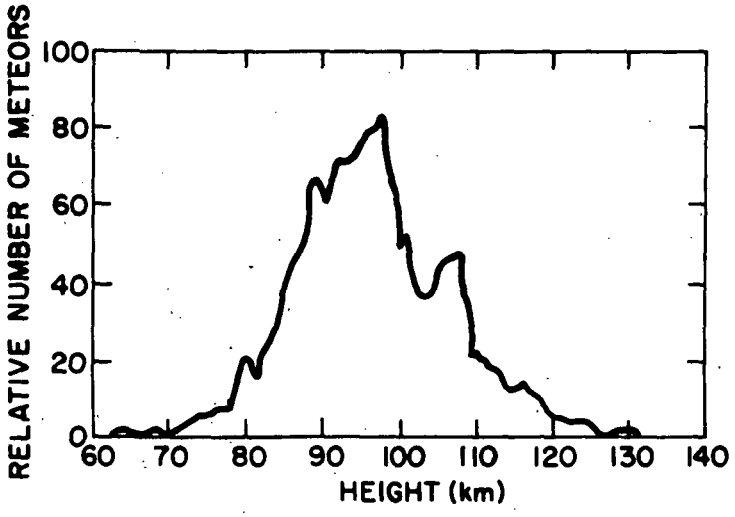

Figure 3.4 Frequency-height distribution of 548 long-enduring echoes observed at Ottawa.

enough so that the incident wave passes through the trail and the trail can be considered as an array of independent scatterers. Overdense trails are those where the electron density is high enough to prevent complete penetration of the incident wave and secondary scattering from electron to electron becomes important. The transition point from underdense is about $q = 10^{14}$ elec/m [*McKinley*, 1961]. Also, the underdense trails have durations of less than about one second while the overdense trails have longer durations. Only radio reflections from underdense trails are discussed here, since they occur with much more frequency than do overdense trails.

Assume the ionized trail is an infinitely long right-circular cylinder of electrons whose diameter is very small compared to the radar wavelength and that the trail electron density is low enough that the incident wave passes through the trail without major modification. Consider the case of specular reflections with the transmitter and receiver at the same location.

The signal received can be computed by summing the energy backscattered by each electron in the trail while taking proper account of the phase relations of these contributions. When this is done it is found that the principal contribution of energy from a trail is from its first Fresnel zone, a region of length $\sqrt{2\lambda R}$ where λ is the wavelength of the transmitted signal and R is the range of the meteor trail reflection. On the rest of the trail echo contributions from neighboring Fresnel zones tends to cancel each other. As the trail expands by diffusion the phase difference of the contributions from the electrons on opposite sides of the trail increases so that the received power decreases.

The transmission equation can be written in terms of the scattering cross section σ in the following way [*Sugar*, 1964]

$$\frac{P_R}{P_T} = \frac{G_T G_R \lambda^2}{16\pi^2 R^4} \sigma \tag{3.1}$$

where

P_T, P_R = the transmitted and the received powers, respectively

G_T, G_R = power gains of the transmitting receiving antennas relative to an isotropic radiator, respectively

λ = wavelength

R = distance from the transmitter to the reflection point

σ = scattering cross section of the trail

If it is assumed that the trail is initially in the form of a line of electrons (an initial radius of zero), the scattering cross section is

$$\sigma = \frac{1}{2} R \lambda r_e^2 q^2 \exp(- \frac{32 \pi^2 D}{\lambda^2} t) \tag{3.2}$$

where

r_e = classical radius of the electron

q = electron line density of the trail

D = diffusion coefficient

t = time measured from the formation of the trail

The first factor in Equation (3.2) represents the scattering cross section of the initial distribution of electrons. The second factor represents the attenuation with time as the trail expands and destructive interference begins. The distribution of electrons across the trail has a Gaussian shape with an effective radius $\sqrt{4Dt}$ [*Kaiser*, 1953]. The signal amplitude, which is proportional to $\sqrt{\sigma}$ will have fallen to $1/e$ of its initial value at the time the radius of the trail is $\lambda/2\pi$.

If the initial radius of the trail is not taken to be zero, the extra attenuation associated with this finite radius may be estimated by assuming that the initial distribution of electrons is Gaussian. Then, the effect of the finite initial radius of the received power is equivalent to a shift in the time scale. Using the relation $r = \sqrt{4Dt}$ and Equation (3.2), the initial attenuation is $\exp(-8\pi^2 r_0^2/\lambda^2)$ where r_0 is the initial radius of the trail. When this effect is included in Equation (3.2) and the result substituted in Equation (3.1), one obtains the following

$$\frac{P_R}{P_T} = \frac{G_T G_R \lambda^3 q^2 r_e^2}{32\pi^2 R^3} \exp\left(-\frac{8\pi^2 r_0^2}{\lambda^2}\right) \exp\left(-\frac{32\pi^2 Dt}{\lambda^2}\right) . \qquad (3.3)$$

Since it was assumed that trails were of inifnite length in the above relation, every trail has a first Fresnel zone and, therefore, gives a specular reflection. In practice, however, since trails are of finite length this zone may not exist on the trail. In such a case the returned signal is weak and is of little importance. Thus, a radar can see only a fraction of all trails incident on the ionosphere because most trails do not have the proper orientation for the line of sight to be perpendicular to the trail.

3.5 *Modifying Effects*

The simple model for the underdense trail that is given above can be used to interpret many observed effects of underdense echoes. For a more detailed picture, however, some further points have to be considered.

A process influencing the plasma of the trail is a loss of electrons through recombination and attachment to neutral molecules. *Deegan et al.* [1970] have observed recombination in their trail data. They have also

shown that the neglect of recombination effects can cause wrong conclusions to be drawn from meteor trail observations.

The effects of ionospheric winds are appreciable for trails which last for the order of a second or more. Trail distortion resulting from wind shears can lead to the formation of several specular reflection points. The received signal is a composite of these contributions. Since each reflection point is moving at a different velocity, the returns from each specular reflection point have different Doppler shift and the resulting composite signal fades in an irregular manner [*Manning and Eshleman*, 1959].

Signal losses through absorption in the *D* region can become quite noticable. This effect disappears at night but can reach a noon maximum of -10 dB at 30 MHz [*Nowak*, 1967]. During ionospheric disturbances, abnormally large values of absorption occur.

The reflection coefficient also depends on the orientation of the trail with respect to the polarization of the radar wave. This is an effect peculiar to the cylindrical geometry of the meteor trail. The transverse component of the electric field polarized the plasma, and if the plasma frequency is $\sqrt{2}$ times the signal frequency, resonance in the trail occurs. For a longitudinal field, this effect is absent because of the lack of boundaries at which polarization may be set up [*Manning and Eshleman*, 1959]. Plasma resonance occurs typically at the beginning of an echo, and enhances it. As the trail expands the transverse reflection coefficient approaches the longitudinal one. Hence, in the beginning of the echo the decay is faster than that given by the simple trail theory. For strong echoes a sudden change in decay rate, occurring as the plasma resonance effect ends, is sometimes observed. Depending on the system sensitivity, however, the signal might

disappear in the noise before the change in decay is obvious. Then, the first part of the echo, with superimposed decays from diffusion and resonance, might be interpreted as stemming from diffusion alone, leading to an error in the determination of the diffusion coefficient.

The measurements of winds, as derived from the radial motion of the reflecting trail point with respect to the radar, is fairly straightforward. It has been shown that the motion of a meteor trail is indeed that of the surrounding atmosphere, since any influence of the earth's magnetic field on trail motions has been discounted by experimental results which showed predominantly horizontal motions in a region where the magnetic dip angle is 65° [*Manning et al.*, 1950]. The measurement of the Doppler shift in the echo, used to determine radial motion of the target, is only invalidated if several reflection points on the trail exist, from which different Doppler shifts are superimposed into a combined waveform. These cases would be accompanied by a corresponding fading in the amplitude record, so these echoes can be identified and eliminated from the data.

4. OBJECTIVES AND TECHNIQUES OF MEASUREMENT

4.1 *Objectives of the System*

It is planned to build and operate a simple and reliable meteor radar system that will be able to measure winds in the altitude region between 80 and 120 km. Especially now, when investigators of the upper atmosphere are trying to extend models for global circulations to high levels, such data are urgently needed above the mesosphere.

Present indications are that the proposed facility should be able to exceed all presently operating meteor radar facilities in performance. This is primarily because of the 4 Mw power of the transmitter to be used. This transmitter and other equipment that formerly comprised the Havana Radio Meteor System has been given to the University of Illinois by the Smithsonian Astrophysical Observatory and the Department of Commerce.

Table 2.1 shows that the power of the Havana transmitter is approximately two orders of magnitude greater than that of other meteor radar facilities. Now the number of meteor trails with an electron line density of q or larger is inversely proportional to q [*Manning and Eshleman*, 1959]. Since the received echo power is proportional to q^2 and the transmitted power (see Equation 3.2), the number of echoes detected above the noise threshold with the Havana transmitter is an order of magnitude greater than the number detected with the other systems (see column 5 of Table 2.1). The high echo rate of the proposed facility makes it possible to obtain wind determinations with improved time and height resolution, permitting the study of motions with short periods and small vertical wavelengths.

One of the most important design considerations for the proposed facility is that the height of the echo should be accurately determined, since the study of gravity waves with realtively high frequencies is a principal objective. These motions are expected to have a small vertical length scale. This fact can be seen from the asymptotic approximation of the dispersion relationship to interval gravity waves (i.e., assuming $K_z^2 >> \omega_a^2/c^2$)

$$K_z^2 = K_x^2 \left[\frac{\omega_B}{\omega^2} - 1\right] \tag{4.1}$$

where

K_x, K_z = horizontal and vertical wave numbers, respectively

ω_a = acoustic frequency = $\frac{\gamma a}{2c}$

ω_B = Brunt-Vaisala frequency for an isothermal atmosphere = $(\gamma - 1)\frac{g^2}{c^2}$

c = speed of sound

γ = ratio of specific heats = $\frac{C_P}{C_V}$

g = gravitational acceleration

If one takes K_x and ω_B to be constants and decreases ω [*Hines*, 1960], K_z must increase, that is, the vertical scale must become small.

The radial wind must be so that the small amplitude oscillations in the meteor region can be detected.

Another important design consideration is simplicity. Some of the shortcomings of the Havana system were an outgrowth of its complexity and the resulting complexity of data analysis. All seven outlying stations had to send phase synchronous data for each pulse back to the main station. There the signals were sent through a series of delay lines and echo-pattern recognizers. All this information eventually ended up in a 18-channel recorder (see Section

2.6). The new facility will utilize one station in finding the velocity and height of a meteor trail echo. Very little hardware equipment is to be placed between the receiver and the recorder. All the processing and echo recognition will be done in the computer. The proposed system is designed with the scientific objectives of wind measurement at the forefront, the aim being to insure routine operation and data analysis within reasonable cost limitations.

The proposed meteor radar facility will be capable of continuously monitoring horizontal wind and perhaps neutral density in the 80-120 km altitude range. From these one will be able to find prevailing winds, tidal oscillations, gravity waves and turbulence. The system requirements for obtaining these different dynamic parameters become progressively more stringent. Gravity waves and turbulence require a height accuracy of $\pm$ 0.5 km and a minimum echo rate of hundreds per hour [*Barnes*, 1968], due to the short vertical length scales and the short time scale of these types of motion. The prime design objective is therefore the capability of the proposed system to observe gravity waves. The high data-collection rate resulting from the power of the new facility makes this a realistic objective.

In summary the objective is to use the high-powered transmitter, together with systems for measuring echo location quite accurately, to study short-time-scale dynamics in the 80-120 km altitude range in a way that no existing facility presently is able. This can be accomplished within state-of-the-art technology.

4.2 *General Approach*

Winds are measured from the Doppler shift of the meteor echo. The measurement of the Doppler shift is outlined in Section 4.3. The height of the echo is determined by its range and elevation angle, which are to be discussed in Section 4.4.

Different meteor radar installations use different methods to measure horizontal wind. For instance, the Garchy system used one transmitter and receiving system to measure the east-west and another to measure the north-south wind. The AFCRL system at Durham is alternately pointed NE and NW to give the two orthogonal wind components. The plan of the Havana system was to measure orthogonal wind components by using a number of outlying receiving stations and hence a number of lines-of-sight.

At Illinois it is planned to use a broad horizontal beam and an interferometer to measure the azimuth angle of the meteor echoes. A similar interferometer system is used to determine the elevation angle. This, along with range information, gives horizontal wind as a function of height with some horizontal averaging implied over the width of the beam. From these wind data the zonal mean wind, planetary waves, tides, gravity waves and turbulence can be studied.

4.3 *Doppler Measurements*

The measurement of wind by a meteor radar is based on the Doppler shift of a meteor echo relative to the transmitted signal. The Doppler frequency is given by Equation (2.2)

$$\Delta f = \frac{2v}{c} f_t \quad . \tag{4.2}$$

This yields the line-of-sight velocity v of the meteor trail which is assumed to result from the neutral wind.

At the University of Illinois the Doppler shift will be obtained by comparing the phase of the received signal with the phase of the transmitted signal. The outputs of a phase comparator will be a sine wave and cosine wave of frequency Δf. By manipulation of the following signals

$$\text{cosine output at time } T_1 = A \cos(-\omega\Delta t + \phi)$$

$$\text{sine output at time } T_2 = A \sin \phi$$

$$\text{cosine output at time } T_3 = A \cos(\omega\Delta t + \phi)$$

where A = amplitude proportional to the strength of the received pulse, $\omega = 2\pi\Delta f$, $\Delta t = T_2 - T_1 = T_3 - T_2$ = time between pulses and ϕ = phase of signal at the antenna, one obtains (Backof and Bowhill, 1972)

$$\sin \omega\Delta t = \frac{\cos(-\omega\Delta t + \phi) - \cos(\omega\Delta t + \phi)}{2 \sin \phi} \quad . \tag{4.3}$$

From sin $\omega\Delta t$, the Doppler frequency can easily be determined. Since sin $\omega\Delta t$ is an odd function, the sense of the drift can be obtained.

4.4 *Range and Angle Measurements*

The height of an echo is obtained from the range and angle of arrival measurements. The range is essentially determined by the number of microseconds between the transmission and reception of a pulse. Since the A/D converter used in this system samples at every 10 μs, the pulse width has to be at least this large. Thus the 3 dB width of the pseudo-guassian pulse is chosen as 10 μs.

Several methods for determining the angle of arrival of an echo are available and are discussed by *Nowak* [1966]. At the new facility in Illinois the angle of arrival is obtained by three receiving antennas arranged in an interometric mode. The antennas will be located at the vertices of a right triangle with one side parallel to the beam axis, to measure both the azimuth and elevation angles. A top view of the receiving array is shown in Figure 4.1.

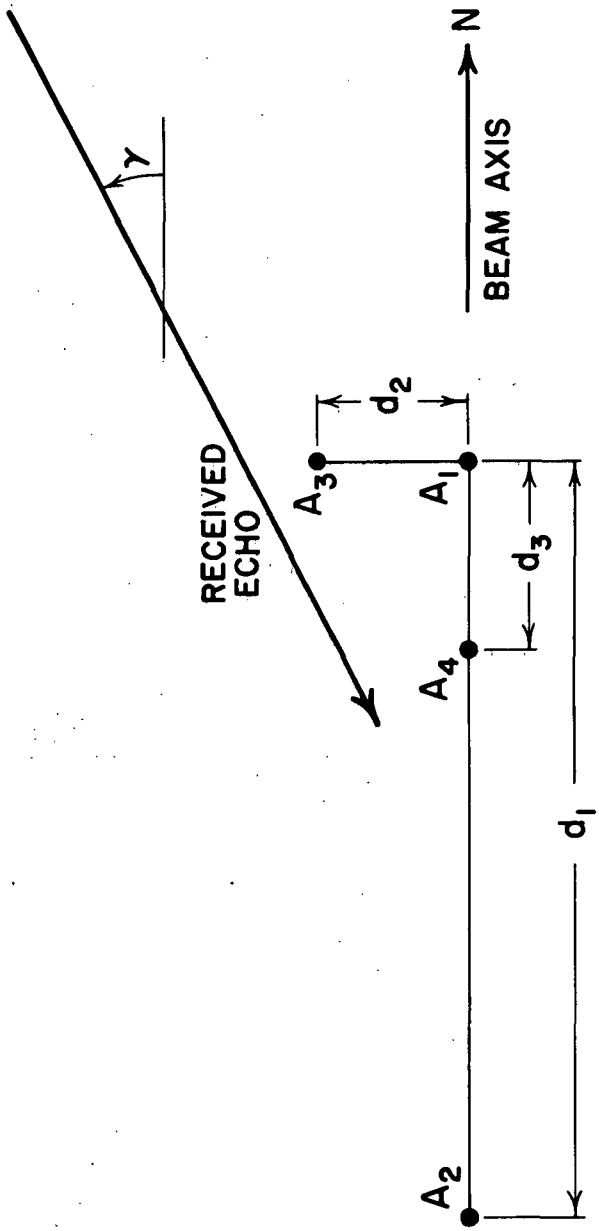

Figure 4.1 Top view of receiving antennas A_1, A_2, A_3 and A_4.

To determine the direction of arrival of the echo, the phase difference Φ_1 between the fields received by the two antennas A_1 and A_2 is determined (see Figures 4.1 and 2.7) by

$$\Phi_1 = \frac{2\pi d_1}{\lambda} \cos \beta = \frac{2\pi d_1}{\lambda} \cos \alpha \cos \gamma \quad . \tag{4.4}$$

The antennas A_1 and A_2 are aligned along the beam axis, which is pointed to the north. For an arbitrary location of the echo, Φ_1 is a function of both the azimuth angle γ and the elevation angle α. The phase difference between A_1 and A_3, which are aligned perpendicular to the beam axis, is also determined where

$$\Phi_2 = \frac{2\pi d_2}{\lambda} \sin \theta = \frac{2\pi d_2}{\lambda} \cos \alpha \sin \gamma \quad . \tag{4.5}$$

The angles β and θ as well as the elevation angle α and the azimuth angle γ are pictured in Figure 4.2 [*Sugar*, 1964].

To avoid ambiguity, the antenna separations d_1 and d_2 have to be chosen so the path length differences Δl_1 and Δl_2 are less than 1λ thus,

$$\Delta l_1 = d_1 \cos \beta < \lambda \quad , \tag{4.6}$$

$$\Delta l_2 = d_2 \sin \theta < \lambda \quad . \tag{4.7}$$

Thus the azimuth separation d_2 is set at 1λ. The elevation separations d_2 can also be set at 1λ to give no ambiguity. But 1λ is too small a value to get the desired measurement accuracy in the elevation angle. Therefore, a fourth

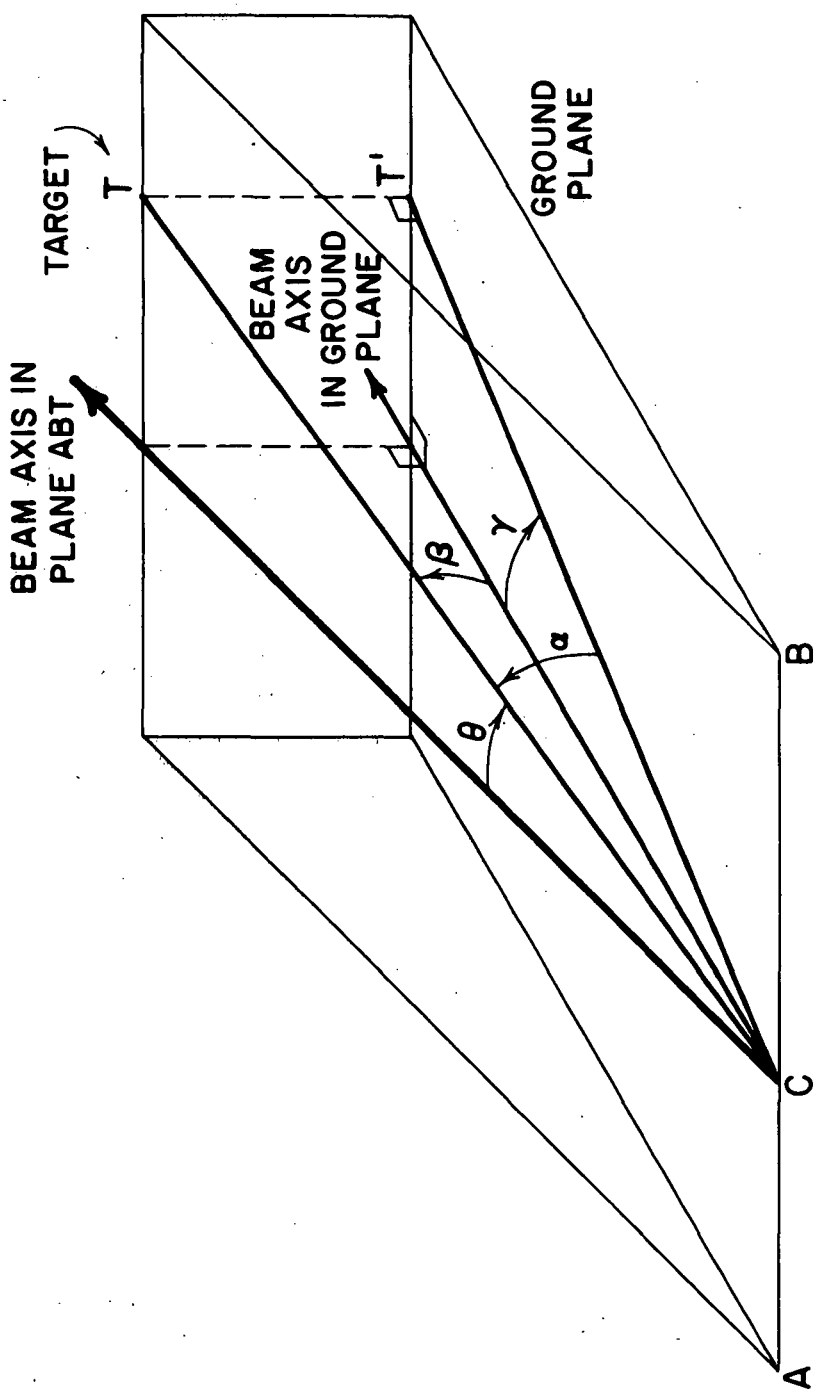

Figure 4.2 Illustration of the various angles of measurement.

antenna is needed. Antenna A_2 is placed 20λ from A_1 to get the measurement accuracy. A_4 is placed 1λ from A_1 along the same axis to resolve any ambiguity.

In summary the Doppler shift is obtained by phase comparison at one receiver. The angle measurement, however, is determined by comparing the phases between pairs of receivers. The range is obtained by timing the transmission and the reception of a pulse. The equipment used for these measurements will be discussed in the next chapter. The accuracies are discussed in Chapter 6.

5. SYSTEM DESCRIPTION

The transmitted beam will cover a large colume at meteor region altitudes. When a meteor trail is oriented at right angle to the beam, an echo is detected by the receiving antenna. From the antenna the echo enters the receiver. The phase of the reflected signal is then compared with the phase of the transmitted signal. Two waves proportional to the sine and cosine of the Doppler frequency are the outputs of the receiver. These outputs along with those from the other receivers are sent to the multiplexer. The multiplexer acts to send the signals one at a time to the A/D converter so that they can be converted to digital signals. The digital signals are then sent on to the computer for processing and storage. In the computer Doppler frequency, range and elevation and azimuth angles are computed in real time and stored on tape for further use. In the following sections the different parts of this system are described in more detail.

5.1 *Transmitter*

The Continental Electronics Manufacturing Company Type PO-830 transmitter [*Deegan et al.*, 1970] originally located at Havana is now being reconstructed for the new facility at the University of Illinois. Its operating frequency is 40.92 MHz. The transmitter characteristics are as follows:

Peak power output	4 Mw
Average power output	20 kW
Pulse waveform	3 μs at 1330 pps to 100 μs at 40 pps
Nominal duty factor	0.004
Power supply requirements	230 v, 3 phase, 60 cps

Power source capacity	200 kv-a
Type of emission	pulsed CW
Output impedance	100 ohms balanced (two 50-ohm unbalanced outputs 180° out of phase)

The transmitted pulse will be quasi-gaussian with a half-power width of 10 μs. Since the average power is 20 kW, the pulse repetition frequency is chosen as 500 pps.

5.2 *Transmitting Antenna*

One of the objectives in the design of the transmitting antenna is to optimize the number of received echoes from meteor trails. This is to facilitate the study of short period wave modes in the upper atmosphere. The transmitting antenna will be pointed 45° above the ground plane and to the north, where meteors occur most often each day [*Villard et al.*, 1955]. The 45° elevation is chosen from the following line of reasoning. If the beam were pointing at a high elevation angle, very few echoes would be received since a meteor would have to be traveling almost horizontally before specular reflection occurred. A low elevation beam would give many meteor echoes but the noise resulting from the closeness of the beam to the ground and the large radial distance to the meteor region would combine to give a large error in the angle measurements.

The simple antenna envisioned at Illinois is composed of two rows of half-wave dipoles. The two rows are paired in a collinear configuration. Each pair of elements are operated in phase, and the direction of maximum radiation is at right angles to the line of the paired elements. Each row is made up of 11 elements. The spacing between adjacent elements is 0.48 λ

causing a phase difference between adjacent elements of 142°. The antenna is pictured in Figure 5.1.

These values are chosen because of the desire to point the beam 45° above the horizon and to have the elevation beamwidth cover the meteor region adequately between 80 and 120 km. This antenna design satisfies these goals quite well. The array factor for linear array of N elements each spaced by a distance d is given by [*Krauss*, 1950]

$$AF = \frac{1}{N} \left| \frac{\sin N \psi/2}{\sin \psi/2} \right| \tag{5.1}$$

where

$$\psi = \frac{2\pi d}{\lambda} \cos \rho + \delta \tag{5.2}$$

and

λ = wavelength of the transmitting beam

ρ = angle between the line of the array and the line from the center of the array to a far point

δ = difference in the transmitting phase of adjacent sources

To ensure that the transmitting beam has only one main lobe, the distance d has to be chosen so that the array factor does not vary by more than one period, that is,

$$d \leq \frac{1}{2} \left(1 - \frac{1}{2N}\right) \lambda \quad . \tag{5.3}$$

From Equations (5.1), (5.2), and (5.3), the values given above can be obtained.

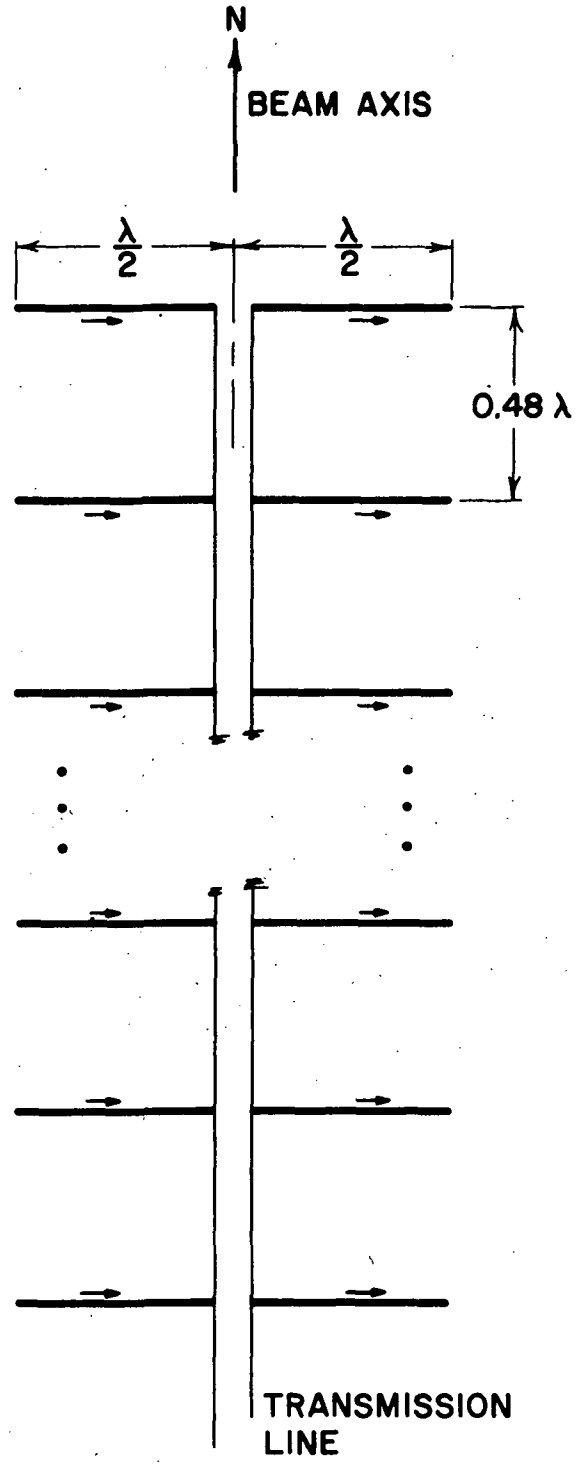

Figure 5.1 The top view of the transmitting antenna. Arrows indicate the direction of positive current flow.

Referring to Figures 5.2 and 5.3, the azimuth beamwidth is 48° and the elevation beamwidth is 11.5°. The gain of this antenna is approximately 17 dB. The wide beamwidth in the azimuth direction is necessary for the determination of both components of the horizontal wind given the planned mode of operation, where only one array of receiving antennas is used to continuously monitor one section of the sky. For example, if Doppler measurements are obtained for trails in the NE and NW directions at about the same height and time, these measurements can be used to give the horizontal wind. The elevation beamwidth is determined by optimizing the meteor region covered by the beam. From symmetry a line of dipole antennas will result in a solid cone-shape beam where the sides of the azimuth pattern curve toward the ground. The transmitted beam should have a rather narrow elevation angle while being rather broad in azimuth. The azimuthal extent of the 3-dB beamwidth in the 80-120 km region is calculated to be 49° while the corresponding elevation extent is 11.6°.

5.3 *Receiving Subsystem*

The receiving antennas that will be used are 13-element Yagi's. The Yagi antennas were manufactured by the Telrex Laboratories of Ashbury Park, New Jersey, and carry model number CY13-40-42. Each Yagi antenna has a 3-dB beamwidth of 30° in the azimuth direction and 64° in the elevation direction. The gain above an isotropic radiator is about 15 dB, and the front-to-back ratio is 30 dB [*Whipple and Hawkins*, 1956]. The Yagi antennas will be mounted on 60-foot poles and pointed north and 45° above the ground plane, centered on the same volume of the sky as the transmitting antenna.

An Aerospace Research Incorporated (ARI) Model PR-40A receiver is connected to each receiving antenna. A block diagram of the ARI receiver is shown in Figure 5.4 [*Deegan et al.*, 1970]. The 40.92 MHz echo returns are converted

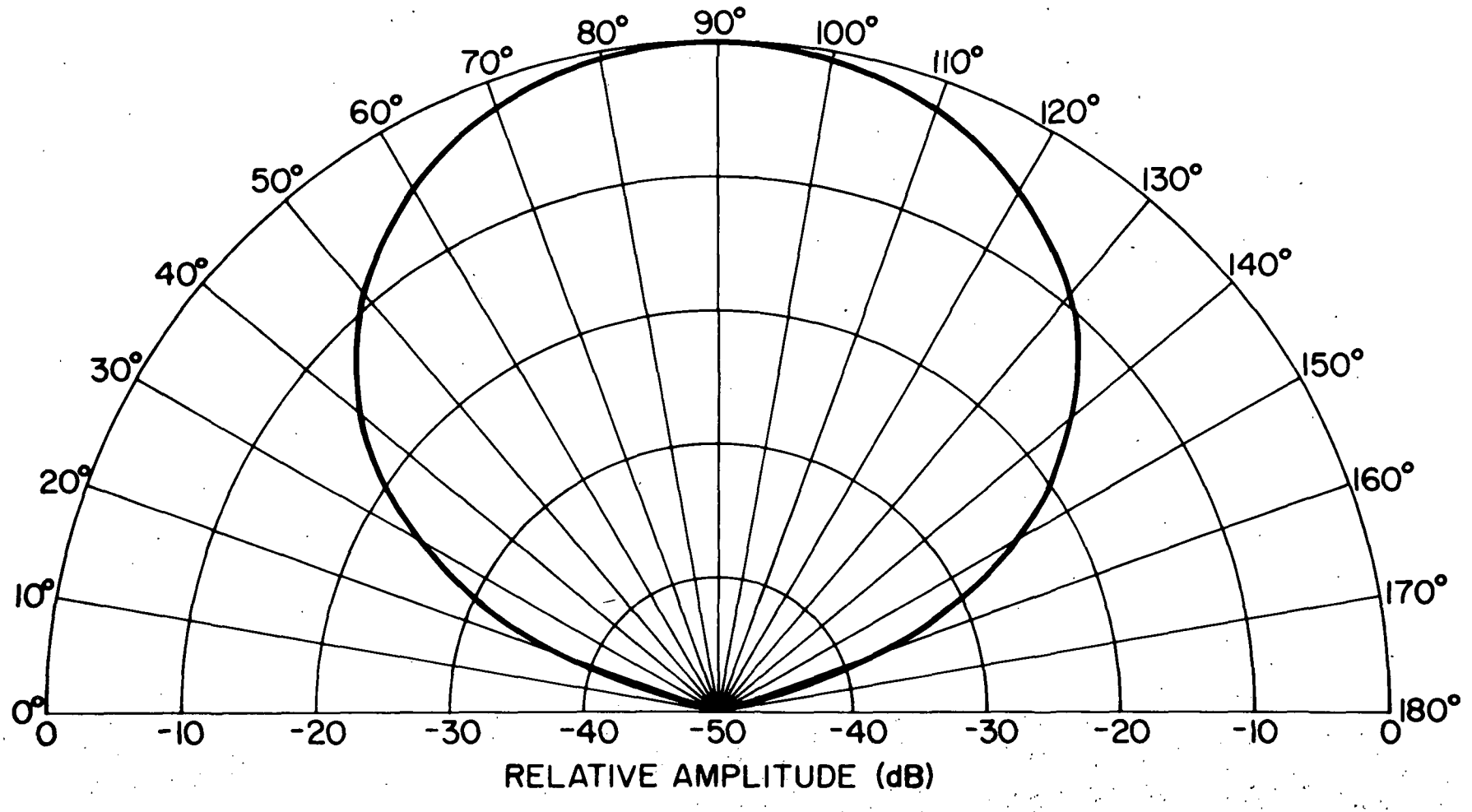

Figure 5.2 Azimuth pattern of transmitting antenna.

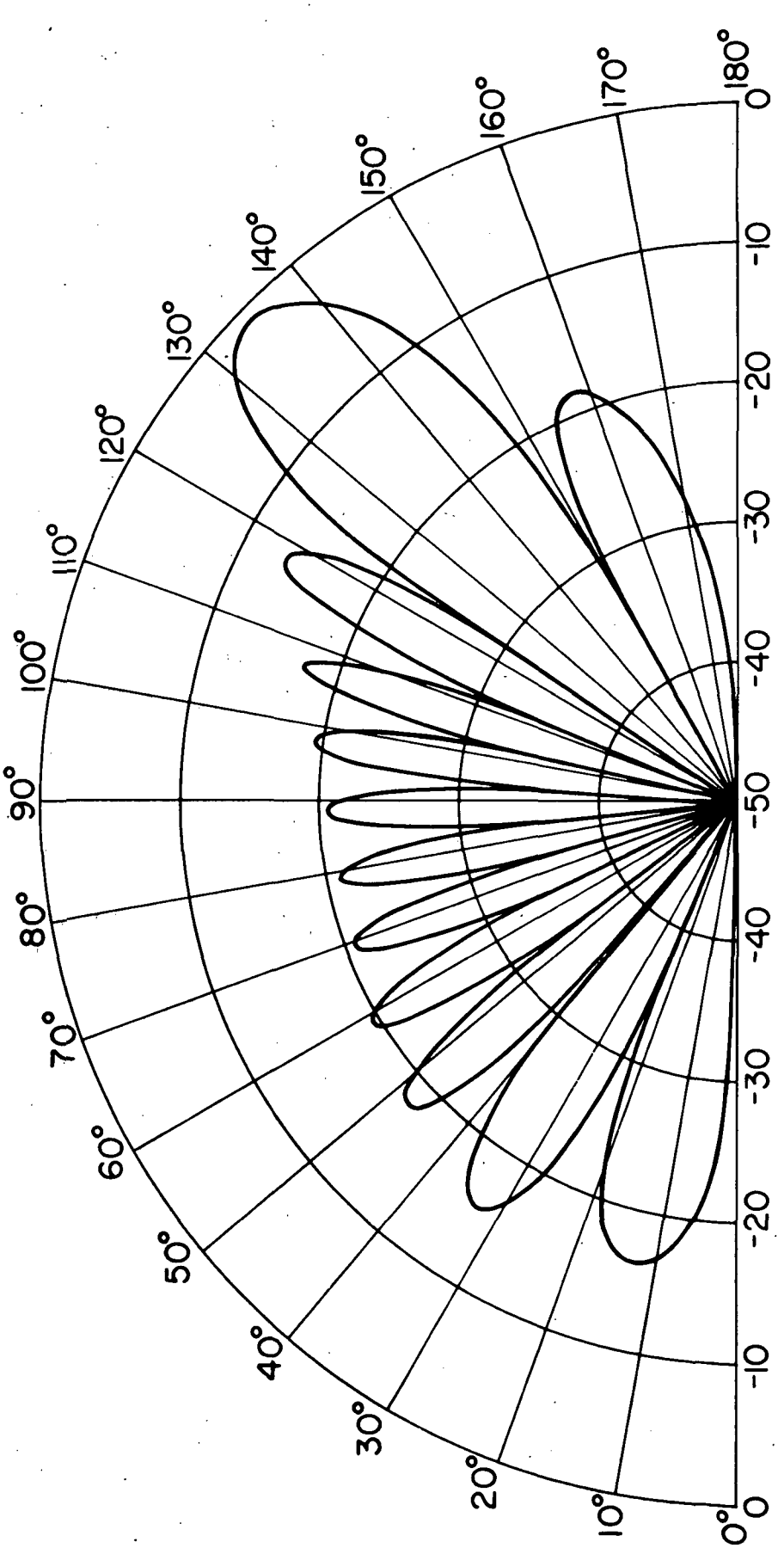

Figure 5.3 Elevation pattern of transmitting antenna.

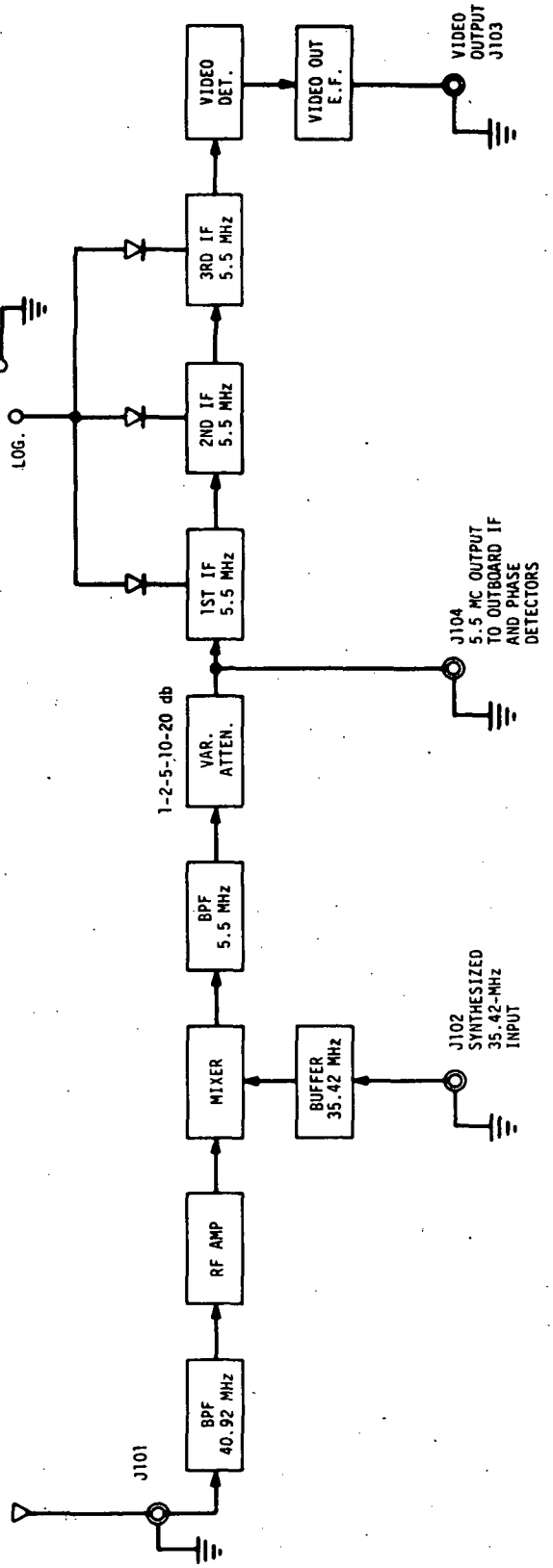

Figure 5.4 Block diagram of the ARI receiver, Model PR-40A.

to the intermediate frequency (IF) of 5.5 MHz, from which are derived both linear and logarithmic video data. The 5.5 MHz signal is also brought to phase detectors for phase comparison measurements. Thus, the outputs of the ARI receiver are an amplitude signal proportional to the amplitude of the echo, and two waves proportional to the sine and cosine of the phase difference $\Delta\phi$ between the return signal and the transmitted signal.

The input-output characteristics and the frequency response of the receiver are shown in Figures 5.5 and 5.6, respectively. The ARI receiver is linear over a range of one decade. The 3-dB bandwidth of the receiver IF output is 180 kHz.

To get an idea of the strength of the received signal, the signal-to-noise ratio from a meteor trail whose electron line density is 5×10^{11} elec/m will be calculated. From Equation (3.3) and the fact that the noise at the antenna is given by $P_N = kT_S B$, the signal-to-noise ratio is

$$\frac{P_S}{P_N} = \frac{G_T G_R \lambda^3 P_T q^2 r_e^2}{32\pi^2 R^3 k T_S B} \exp\left(-\frac{8\pi^2 r_0^2}{\lambda^2}\right) \tag{5.4}$$

where

G_T = gain of the transmitting antenna

G_R = gain of the receiving antenna

λ = wavelength of the transmitting signal

P_T = power of transmitting signal

q = electron line density

r_e = classical radius of the electron

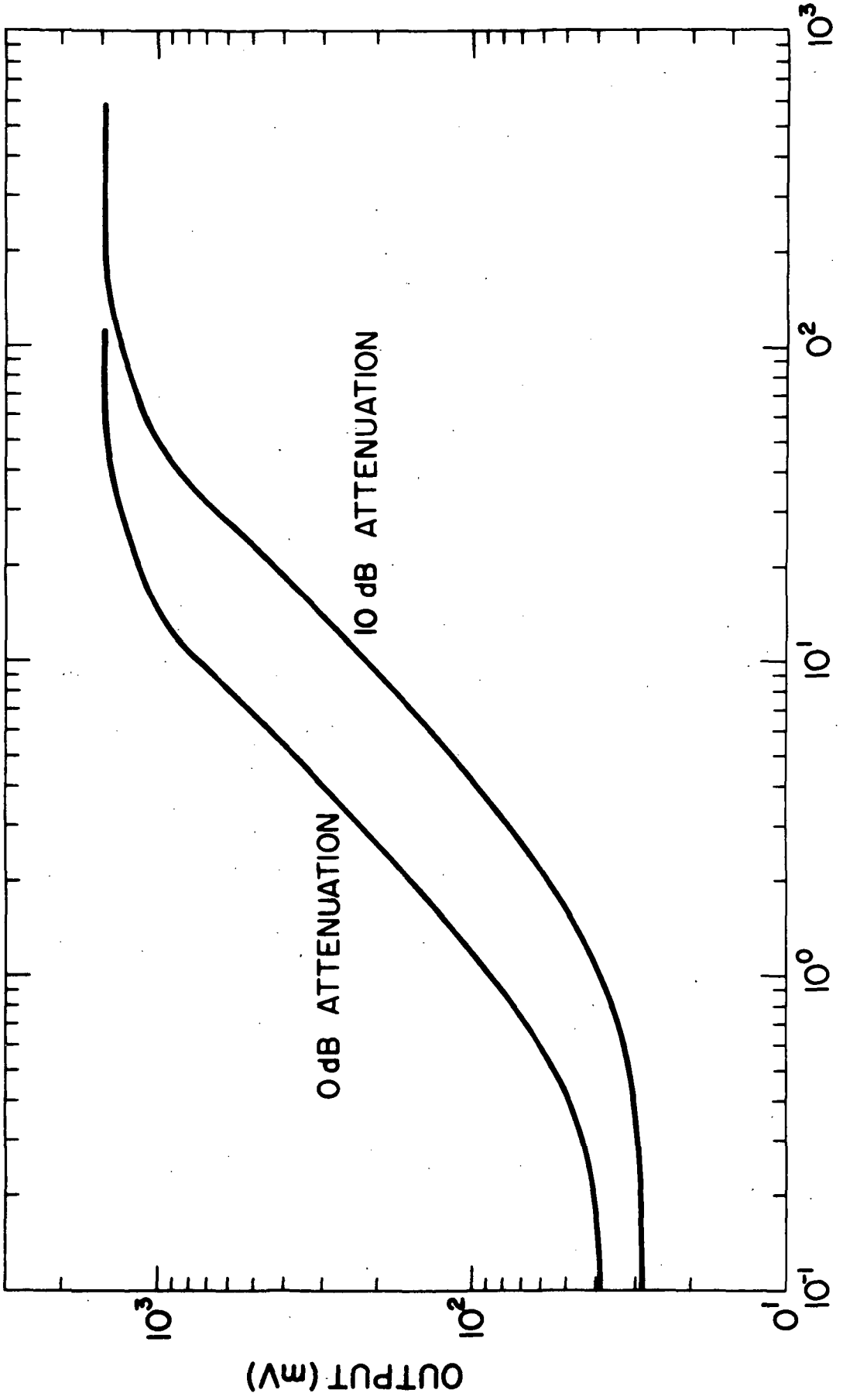

Figure 5.5 Input vs output characteristic of the ARI receiver.

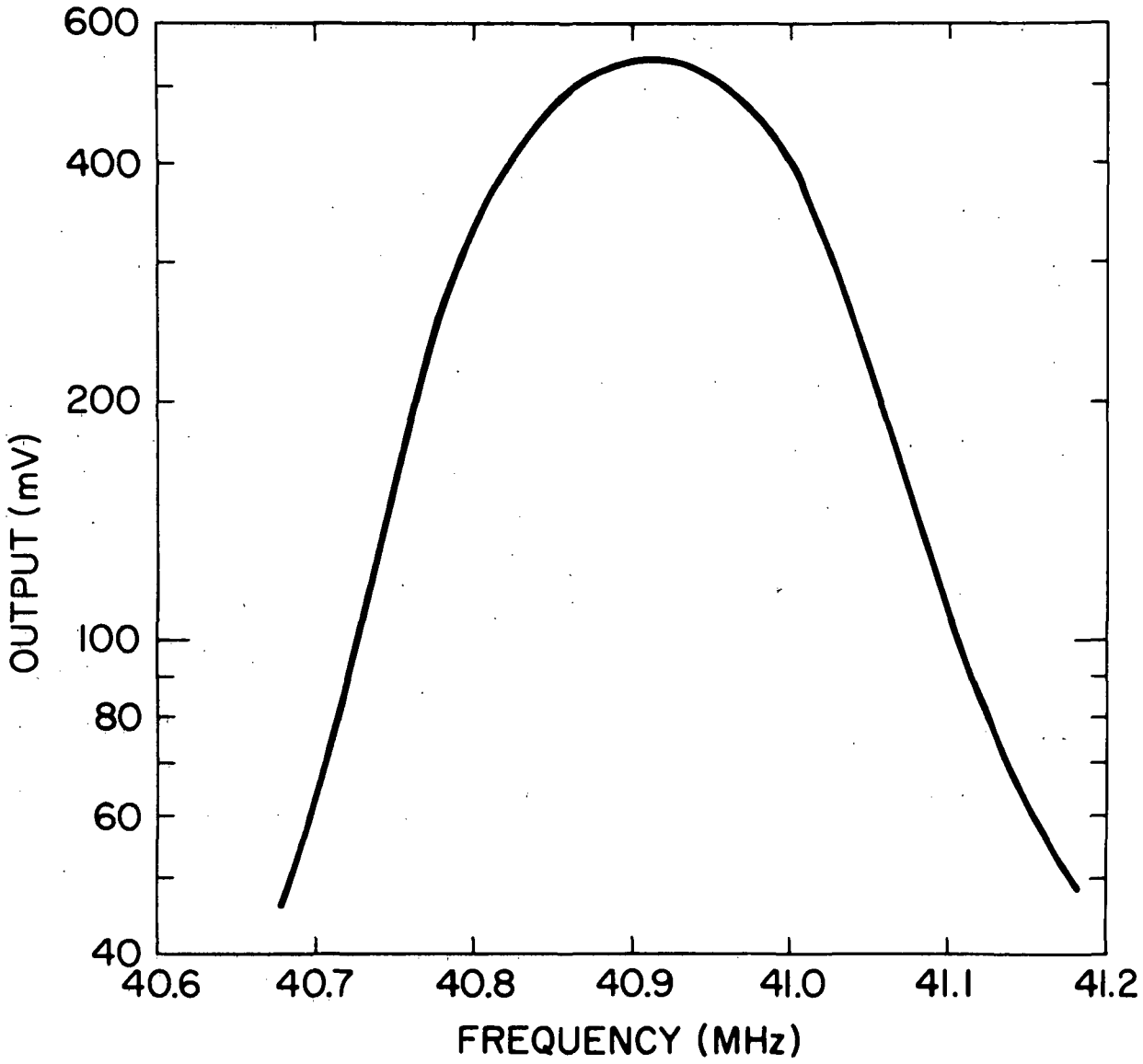

Figure 5.6 Frequency response of the ARI receiver.

R = line-of-sight distance from the transmitter to the trail

k = Boltzmann constant

T_S = antenna temperature due to noise

B = receiver bandwidth

r_0 = initial radius of the trail

The dominant noise is the system is the sky noise, which is chosen as $10^4 °K$ [*McKinley*, 1961]. Thus, if the initial radius of the trail is 1 m, the signal-to-noise ratio is about 17 dB.

To determine the sensitivity of the system, the expected hourly rate of the meteors will be calculated. *Manning and Eshleman* [1959] have estimated the number n of trails per square meter per second n with an electron line density of q or greater by

$$n = \frac{160}{q} \quad . \tag{5.5}$$

For $q = 10^{11}$ elec/m and the collecting area in the meteor bounded by the half power points of the antenna equal to 5600 sq. km, the number of meteor trails seen per hour is 32,000. About 10% of these will have the proper orientation for reflection [*Whipple and Hawkins*, 1956] so that 3200 trails should be received per hour by the Illinois system.

5.4 *Digital Recording and Reduction*

All of the processing and recording of the return echoes from meteor trails will be done by a PDP-15 computer. The computer has a cycle time of 800 ns, implying that the maximum instruction rate is about 10,000 per second in a high level language. After reduction the wind data will be recorded on DEC-tapes.

The meteor radar reduction program will determine in real time the Doppler shift, the range and the elevation and azimuth angles of the echoes. From this information the computer changes the spherical coordinates of the reflection point into cartesian coordinates and the radial drift velocity is calculated from the Doppler shift. The location and velocity of the trail are then recorded on magnetic tape for more elaborate reduction at some later time. *Backof and Bowhill* [1972] have studied this reduction procedure in detail. A summary of their work will be presented here.

The reduction of the Doppler shift has already been discussed in Section 4.3. Equation (4.2) is rewritten here.

$$\sin \omega\Delta t = \frac{\cos(\omega\Delta t - \phi) - \cos(\omega\Delta t + \phi)}{2 \sin \phi} \quad . \tag{5.6}$$

Since the denominator of the expression can take on the value of zero, singularities must be considered. If a fourth measurement

$$\text{sine output at time } T_4\text{: } A \sin(2\omega\Delta t + \phi)$$

is added, then $\sin \omega\Delta t$ is also given by

$$\sin \omega\Delta t = \frac{\sin(2\omega\Delta t + \phi) - \sin \phi}{2 \cos(\omega\Delta t + \phi)} \quad . \tag{5.7}$$

If the denominator of Equation (5.6) is small, then the denominator of Equation (5.7) is large by comparison, and vice versa. Thus the expression with the larger denominator is chosen for the calculation of the Doppler shift.

To determine the range, one of the receivers is chosen as the reference. When a pulse is transmitted, the amplitude output of the reference receiver is simultaneously sent through the multiplexer to the A/D converter. The A/D converter samples the amplitude signal at every 10 μs, and the digitized signal is recorded in the core memory of the computer. The sampling and storing continues for 1.3 ms, corresponding to a maximum range of reflection of 200 km. The 130 core locations which are filled are then searched for the peak value. The location of this memory word relative to the first memory word indicates the value of the range.

In order to determine the elevation and azimuth angles of arrival, three phase comparisons are made (see Section 4.4). Since the three measurements--fine elevation, course elevation and azimuth--are similar, they will be treated as one here. If the sine and cosine outputs at one receiver are measured, followed by the measurements of the sine and cosine at a second receiver, then a trigonometric manipulation of these four quantities can be accomplished to obtain the phase difference. *Backof and Bowhill* [1972] have shown that the following four measurements

$$\text{from antenna \#1 at } t_1\text{: } M_1 = A_1 \sin(\phi_1 + \omega t_1)$$

$$\text{from antenna \#1 at } t_2\text{: } M_2 = A_1 \cos(\phi_1 + \omega t_2)$$

$$\text{from antenna \#2 at } t_3\text{: } M_3 = A_2 \sin(\phi_2 + \omega t_3)$$

$$\text{from antenna \#2 at } t_4\text{: } M_4 = A_2 \cos(\phi_2 + \omega t_4) \ ,$$

where

A_1, A_2 = amplitude factors at receivers #1 and #2, respectively

$\phi_1+\phi_2$ = phase constants at receivers #1 and #2, respectively

ω = doppler frequency

can be manipulated to give

$$\sin(\phi_1 - \phi_2) = \frac{x}{\sqrt{x^2 + y^2}} \tag{5.8}$$

and

$$\cos(\phi_1 - \phi_2) = \frac{y}{\sqrt{x^2 + y^2}} \tag{5.9}$$

where

$$x = (M_1M_3 + M_2M_4) \cos 2\rho - M_1M_4 \sin\rho + M_2M_3 \sin 3\rho$$

$$y = (M_1M_3 + M_2M_4) \sin 2\rho + M_1M_4 \cos\rho - M_2M_3 \cos 3\rho$$

$$\rho = \omega(t_2 - t_1) = \omega(t_3 - t_2) = \omega(t_4 - t_3) \quad .$$

The value of ω is taken to be known from the Doppler measurement. Singularities occur only if $\cos\rho = 0$. This corresponds to a radial velocity of 400 m/s, which is an improbable value for the wind in this atmospheric region.

In order to measure all the parameters associated with each meteor trail, a sequence of 16 measurements must be formulated which will input all the phase and amplitude information that are necessary for reduction through the 16-channel multiplexer. The sequence allows multiple measurements of range and Doppler shifts, since these parameters are so important to the accuracy of the calculation.

6. MEASUREMENT ACCURACIES

6.1 *Velocity of the Wind*

There is a quantization error inherent in the measurement of the doppler shift using an A/D converter whose outputs are only integral values between -512 and 511. *Backof and Bowhill* [1972] have shown that the error of $\sin(\omega\Delta t)$ is approximately

$$d(\sin \omega\Delta t) = \left|\frac{\sin \omega\Delta t + 1/2}{A \sin \phi}\right| \text{ for } A \sin \phi \text{ large} \qquad (6.1)$$

where

ω = Doppler frequency

Δt = period of a pulse

A = amplitude factor

ϕ = phase constant

Then the error of the wind velocity v due to trucation is

$$dv = \frac{\lambda}{\cos(\omega\Delta t)\ 4\ \ t}\ \left|\frac{\sin \omega\Delta t + 1/2}{A \sin \phi}\right| \qquad (6.2)$$

where λ is the wavelength of the transmitting signal. The error of the wind is strongly dependent on the amplitude factor $|A|$, which is taken to vary between 10 and 512. Letting $|A| = 400$, $\phi = \pi/2$ and $v = 100$ m/s, the error is $\pm$ 0.65 m/s.

Since the Doppler frequency is calculated from the sine and cosine of the phase difference $\Delta\phi$, another limit on the wind accuracy is the phase stability

per pulse which is about 0.01 rad, caused mainly by noise. This gives a wind error due to noise at ± 2.9 m/s. Thus the total wind accuracy is about ± 3.5 m/s per pulse. If several wind measurements are obtained from the same trail over a short period of time, the measurements can be averaged to get a greater accuracy.

6.2 *Range*

Since the range is determined by the time between the transmission and reception of a pulse, the range accuracy is determined by the length of the pulse, which is 10 μs. If the center of the pulse is taken as reference, the range accuracy is ± 750 m.

If the maximum value that is found in the search of 130 core locations and the two values adjacent to the maximum are considered and the shape of the output pulse is known, then the range can be determined more accurately [*Backof and Bowhill*, 1972]. The ratio of the maximum value to the higher of the two adjacent values is compared to a table of ratios taken from the actual pulse shape. The location of pulse maximum relative to that of sampled maximum can be determined. This technique can effectively improve range accuracy by a factor of 5, or to ± 150 m.

There is also an error in the range due to the noise. This is an error introduced by the fact that there is a finite rise-time. The uncertainty in time is

$$\Delta T_R = \frac{T_R}{S/N} \tag{6.3}$$

where T_R is the rise-time and S/N is the signal-to-noise ratio [*Barnes and Pazniokas*, 1968]. The rise-time T_R is related to the bandwidth BW by the

following [*Van Valkenburg*, 1964]:

$$T_R = \frac{\pi}{BW} \quad . \tag{6.4}$$

Since the receiver bandwidth is 180 kHz, the rise-time is 17.5 μs. For S/N = 15 dB, ΔT_R is .554 μs. Thus the range error due to noise is ± 83 m. The total range accuracy is than about ± 230 m.

6.3 *Elevation and Azimuth Angles*

The angle determinations are obtained assuming that the Doppler frequency ω is known. Thus the error in the Doppler gives rise to an error in the angles of arrival. From Equation (5.8), *Backof and Bowhill* [1972] have shown that the phase error due to the Doppler inaccuracy is 0.02 rad. Including the phase error due to noise, the total phase instability $d\Phi$ is ± 0.03.

The accuracies of the elevation and the azimuth angles of arrival are calculated from Equations (4.4) and (4.5). From those two equations, one gets

$$\frac{\Phi_2}{\Phi_1} = \frac{d_2}{d_1} \tan \gamma \quad . \tag{6.5}$$

Now, the azimuth error is

$$d\gamma = \frac{\partial \gamma}{\partial \Phi_1} d\Phi_1 + \frac{d\gamma}{d\Phi_2} d\Phi_2 \quad . \tag{6.6}$$

Assuming that both measurements Φ_1 and Φ_2 are made with the same error $d\Phi$, one differentiates Equation (6.5) and substitutes into Equation (6.6) to get

$$|d\gamma| = \frac{\cos^2\gamma |d\Phi| d_1}{\Phi_1 d_2} \left(1 + \frac{\Phi_2}{\Phi_1}\right) \quad . \tag{6.7}$$

Remembering that $d_1 = 20\lambda$ and $d_2 = 1\lambda$ and letting $\gamma = 15°$, $\alpha = 45°$ and $d\Phi = 0.03$ rad, the azimuth error becomes

$$|d\gamma| = 6.61 \times 10^{-3} \text{ rad} \quad .$$

Again from Equation (4.4), one obtains

$$\cos \alpha = \frac{\Phi_1 \lambda}{2\pi d_1 \cos \gamma} \quad . \tag{6.8}$$

The elevation error is

$$d\alpha = \frac{\partial \alpha}{\partial \phi_1} d\Phi_1 + \frac{\partial \alpha}{\partial \gamma} d\gamma \quad . \tag{6.9}$$

Differentiating Equation (6.8), one gets

$$|d\alpha| = \frac{\lambda}{2\pi d_1 \sin \alpha \cos \gamma} \left(1 d\Phi_1| + \Phi_1 \tan \gamma \, |d\gamma|\right) \quad . \tag{6.10}$$

Let $d\Phi_1 = 0.03$ rad, $\alpha = 45°$ and $\gamma = 15°$. The elevation error becomes

$$|d\alpha| = 2.12 \times 10^{-3} \text{ rad} \quad .$$

The height accuracy can now be computed. The height h is given by

$$h = R \cos \alpha \tag{6.11}$$

so that the height error is

$$dh = \frac{\partial h}{\partial R} dR + \frac{dh}{d\alpha} d\alpha \quad . \tag{6.12}$$

Differentiating Equation (6.11), one gets

$$|dh| = \sin \alpha |dR| + R \cos \alpha |d\alpha| \quad . \tag{6.13}$$

From previous calculations, the range error dR was shown to be $\pm$ 230 m and the elevation error $d\alpha = 2.12 \times 10^{-3}$ rad. Letting $\alpha = 45°$ and $R = 141$ km, one obtains a height error of

$$|dh| = 375 \text{ m.}$$

The Fresnel zone is given by $\sqrt{2\lambda R}$. If the meteor trail is oriented 45° with respect to the horizontal plane, the height error caused by the averaging over the Fresnel zone is $\pm$ 510 m. Thus the height error due to the phase instability is less than that caused by the finite extent of the Fresnel zone.

7. CONCLUSIONS

7.1 *Fulfillment of the Objectives*

It is desired to build and operate a relatively simple and reliable meteor radar facility at the University of Illinois to measure the wind in the 80-120 km altitude region. Stringent design criteria are imposed on the design of this facility since a principal objective will be to study the shorter period wave phenomena in the upper atmosphere. It is expected that this facility will exceed all other presently operating facilities in performance.

Certainly this meteor wind facility should utilize the 4-Mw transmitter so that the number of useful meteor echoes over the 80-120 km altitude range is maximized. The transmitting antenna is designed to emit a beam that is wide in the azimuth direction and to adequately cover the altitude range of the meteor region and, of course, to have high gain. Because of the large collecting area of this beam and the high transmitted electromagnetic field, more than 3200 meteor trails per hour are expected to be received by the receiving antennas. Also, the transmitting and receiving antennas are pointed north, where the maximum number of meteor trails should be observed over a complete day's observations.

The scientific objectives of the facility dictate that the height of the meteor echo should be as accurately determined as possible, perferably so that the height error is less than altitude interval subtended by the Fresnel zone around the specular reflection point. To do this the range and the elevation angle of the received echo must be determined very accurately. For the range determination, the desired accuracy is attainable by using an

appropriate data reduction procedure. The sampled maximum of the received pulse is compared with the actual shape of the pulse in the data reduction software. This results in a range accuracy of $\pm$ 230 m. The desired accuracy in the elevation angle can be obtained by measuring the azimuth angle as well as the elevation angle. Also, the separation between two receiving antennas aligned along the beam axis is made very large (20 wavelengths). The elevation angle accuracy measured in this manner is $\pm$ 2.12 x 10^{-3} rad, or about $\pm$ 0.12 deg. The height accuracy is then $\pm$ 375 m.

Another important design cirterion is that the error in the determination of the radial wind be small. By using an appropriate method of data analysis, the radial wind accuracy is calculated to be $\pm$ 3.5 m/s. It is possible to get 16 wind measurements from the same trail in 0.3 seconds; thus the measurements can be averaged to get a radial wind accuracy of $\pm$ 0.9 m/s.

A final design consideration is simplicity. Very little hardware equipment is used between the receiver and the computer. All data reduction is done in software. The lack of hardware in the receiving subsystem reduces the need for maintenance and permits changes in the reduction procedure to be made quickly, since changes can be accomplished by altering the software routines.

7.2 *Prospects for Future Work*

The transmitting antenna to be installed at the new facility emits a beam that is quite wide in the azimuth direction. This beam permits the measurement of the two-dimensional horizontal wind. In the future another transmitting antenna may be built with a narrow beam in the azimuth direction. This narrow beam might help to define the azimuth angle very accurately and make possible more extensive sutides of wind shears and gravity waves along a vertical column.

At the present time, all the antennas are designed to point north. This configuration will measure the north-south component of the wind most accurately. Another set of antennas might be built which point toward the east (or west) so that the east-west component of the wind can be determined with comparable accuracy.

In the future, more attention might be given to measuring the amplitude decay of the meteor trails so that the diffusion constant and the density of the atmosphere can be determined. The values measured using this technique could then be compared with those obtained from the incoherent-scatter system being built at Illinois.

A multistatic system could be built in which several other receiving sites are used to measure the wind, thus allowing measurements to be made at more than one specular reflection point on a given trail.

These possible future developments should await examination of the data from the meteor radar facility as it is presently conceived. This should help to point the way to the alternative models of operation that are of most scientific interest.

REFERENCES

Backof, C. A. and S. A. Bowhill (1972), Private communication.

Barnes, A. A., Jr. (1968), Winds and densities from radar meteor trail returns, 80-120 km, Met. Monog., 9, 190-195.

Barnes, A. A., Jr. and J. J. Pazniokas, eds. (1968), Proceedings of the workshop on methods of obtaining winds and densities from radar meteor trail returns, Special Rep. 75, AFCRL-68-0228, Air Force Cambridge Res. Labs., Bedford, Mass.

Chapman, S. and R. S. Lindzen (1970), Atmospheric Tides, Reidel, Dordrecht.

Clark, R. R., F. H. Glanz and A. D. Frost (1970), Satellite verification of an interferometric direction finder for meteor radar echoes, Sci. Rep. 3, F19628-67-C-0230, Ant. Sys. Lab., Univ. New Hampshire.

Deegan, N. R., R. J. Fitzpatric, G. Forti, M. D. Grossi, M. R. Schaffner and R. B. Southworth (1970), Study of meteor wind measurement techniques, Final Rep. 1, AF19-628-3248, Smith. Astrophys. Obser., Cambridge, Mass.

Elford, W. G. and D. S. Robertson (1953), Measurements of winds in the upper atmosphere by means of drifting meteor trails, J. Atmos. Terr. Phys., 4, 271-284.

Eshleman, V. R. (1957), The theoretical length distribution of ionized meteor trails, J. Atmos. Terr. Phys., 10, 57-72.

Fraser, G. J. (1967), Seasonal variation of southern hemisphere mid-latitude winds at altitudes of 70-100 km, J. Atmos. Terr. Phys., 30, 707-719.

Frost, A. D. and R. R. Clark (1970), Antenna radio calibration for the AFCRL meteor radar using OV1-17, Sci. Rep. 2, F19628-67-C-0230, Ant. Sys. Lab., Univ. New Hampshire.

Glass, M., I. Revah and A. Spizzichino (1970), Radars meteoriques mobiles pour l'etude des vents dans la haute atmosphere, Note Tech. EST/RSR/47, Centre National D'etudes Des Telecommunications.

Greenhow, J. S. (1954), Systematic wind measurements at altitudes of 80-100 km using radio echoes from meteor trails, Phil. Mag., 45, 471-490.

Groves, G. V. (1959), A theory for determining upper-atmospheric winds from radio observations on meteor trails, J. Atmos. Terr. Phys., 16, 344-359.

Guha, D. and M. A. Geller (1972), Computer simulation of the three-receiver drift experiment, Aeron. Rep. 50, Aeron. Lab., Univ. of Illinois, Urbana, Ill.

Hawkins, G. S. (1956), A radio survey of sporadic meteor radiants, Monthly Notices Roy. Astron. Soc., 116, 92-104.

Hawkins, G. S. (1963), The Harvard radio meteor project, Proc. of the Symposium on the Astronomy and Physics of Meteors, Smith. Contr. Astrophys. 7, Washington, D. C.

Hines, C. O. (1960), Internal gravity waves at ionospheric heights, Can. J. Phys., 38, 1441-1481.

Justus, C. G. (1967), The eddy diffusion, energy balance parameters, and heating rate of upper atmospheric turbulence, J. Geophys. Res., 72, 1035-1039.

Kaiser, T. R. (1953), Radio echo studies of meteor ionization, Advan. Phys., 2, 495-544.

Kraus, J. D. (1950), Antennas, McGraw-Hill Co., New York.

Manning, L. A., O. G. Villard, Jr. and A. M. Peterson (1950), Meteoric echo study of upper atmosphere winds, Proc. IRE, 38(8), 877-883.

Manning, L. A. and V. R. Eshleman (1959), Meteors in the ionosphere, Proc. IRE, 47, 186-199.

McKinley, D. W. R. (1961), Meteor Science and Engineering, McGraw-Hill Co., New York.

Mitra, S. K. (1947), The upper atmosphere, Roy. Asiatic Soc. Bengal Monog. Ser., V.

Mitra, S. K. (1949), A radio method of measuring winds in the ionosphere, Proc. IEE, 43, 441-446.

Muller, H. G. (1970), The Sheffield meteor wind experiment, Quart. J. Roy. Meteor. Soc., 96(408), 195-213.

Nowak, R. (1967), An integrated meteor radar system for wind and density measurements in the upper atmosphere, Final Report, AFCRL-67-0347, Stn. Elec. Lab., Stan. Univ.

Nowak, R. (1966), Height determination of radar echoes from meteor trails, Sci. Rep. 3, AFCRL-67-0108, Stan. Elec. Labs., Stan.

Nowak, R., E. M. North and M. S. Frankel (1970), The Stanford meteor-trails radar Mark II, Final Rep., AFCRL-70-0365, Stan. Elec. Lab., Stan. Univ.

Spizzichino, A. (1969a), Etude des interactions entre les differentes composante du vent dans la haute atmosphere, Ann. Geophys., 25(3), 693-695.

Spizzichino, A. (1969b), Etude experimentale des vents dans la haute atmosphere, I, Ann. Geophys. 25, 697-720.

Spizzichino, A. (1969c), Etude des interactions entre les differentes composantes du vent dans la haute atmosphere, II, Ann. Geophys. 25, 755-771.

Spizzichino, A. (1969d), Étude des interactions entre les différentes composantes du vent dans la haute atmosphère, III, Ann. Geophys. 25, 773-783.

Spizzichino, A. (1970a), Étude des interactions entre les différentes composantes du vent dans la haute atmosphère, IV, Ann. Geophys. 25, 9-16.

Spizzichino, A. (1970b), Étude des interactions entre les différentes composantes du vent dans la haute atmosphère, V, Ann. Geophys. 25, 25-34.

Spizzichino, A., J. Delcourt, A. Giraud and I. Revah (1965), A new type of continuous wave radar for the observation of meteor trails, Proc. IEEE, 53(8), 1084-1086.

Sugar, G. R. (1964), Radio propagation by reflection from meteor trails, Proc. IEEE, 52(2), 116-136.

Van Valkenburg, M. E. (1964), Network Analysis, Prentice-Hall, Inc., Englewood Cliffs, New Jersey.

Villard, O. G., Jr., V. R. Eshleman, L. A. Manning and A. M. Peterson (1955), The role of meteors in extended-range VHF propagation, Proc. IRE, 143(10), 1473-1481.

Whipple, F. L. and G. S. Hawkins (1956), The Harvard radio meteor project, a revised edition of the Final Summary Report of August 16, 1955, AFCRL(122)-458.